

One-sentence summary: A mechanism that enables T cells and amoebae to maintain appropriate population sizes is revealed.

**Editor's summary:**

**Crowd control with coronins**

Peripheral naïve T cells are maintained at near constant numbers. Ndinyanka Fabrice *et al.* uncovered a pathway involving the transmembrane protein coronin 1 in regulating T cell population homeostasis. Coronin 1 abundance correlated with T cell density and was higher in the high T cell density environments of the lymph nodes and spleens. Below threshold densities of T cells, coronin 1 suppressed apoptosis through intracellular retention of surface adhesion molecules. Above threshold densities, coronin 1 abundance was not sufficient to prevent the surface presentation of adhesion molecules and apoptosis. A similar mechanism operated in the amoeba *Dictyostelium discoideum* that depended on a coronin 1 homolog. Thus, T cells and amoebae intrinsically sense and regulate their population densities through cell density-dependent regulation of coronin abundance that in turn modulates apoptosis.

**An evolutionarily conserved coronin-dependent pathway defines cell population size**

Tohnyui Ndinyanka Fabrice<sup>1</sup>, Christelle Bianda<sup>1</sup>, Haiyan Zhang<sup>1</sup>, Rajesh Jayachandran<sup>1</sup>, Julie Ruer-Laventie<sup>1</sup>, Mayumi Mori<sup>1</sup>, Despina Moshous<sup>2</sup>, Geoffrey Fucile<sup>3</sup>, Alexander Schmidt<sup>1</sup> and Jean Pieters<sup>1\*</sup>

<sup>1</sup>Biozentrum, University of Basel, 4056 Basel, Switzerland, <sup>2</sup>Pediatric Immunology, Hematology and Rheumatology Unit, Necker-Enfants Malades University Hospital, Assistance Publique-Hôpitaux de Paris and Imagine Institute, INSERM UMR1163, Université de Paris, 75015, Paris, France and <sup>3</sup>SIB Swiss Institute of Bioinformatics, sciCORE Computing Center, University of Basel, 4056 Basel, Switzerland

\* Correspondence should be addressed to:

Email: [jean.pieters@unibas.ch](mailto:jean.pieters@unibas.ch)

**Abstract**

Maintenance of cell population size is fundamental to the proper functioning of multicellular organisms. Here, we describe a cell-intrinsic cell density–sensing pathway that enabled T cells to reach and maintain an appropriate population size. This pathway operated “kin-to-kin” or between identical or similar T cell populations occupying a niche within a tissue or organ, such as the lymph nodes, spleen, and blood. We showed that this pathway depended on the cell density-dependent abundance of the evolutionarily conserved protein coronin 1, which coordinated prosurvival signaling with the inhibition of cell death until the cell population reached threshold densities. At or above threshold densities, coronin 1 expression peaked and remained stable, thereby resulting in the initiation of apoptosis through kin-to-kin intercellular signaling to return the cell population to the appropriate cell density. This cell population size-controlling pathway was conserved from amoeba to humans, thus providing evidence for the existence of a coronin-regulated, evolutionarily conserved mechanism by which cells are informed of and coordinate their relative population size.

## Introduction

All multicellular organisms require a mechanism to regulate the appropriate numbers of cells within their tissues. Various processes have been described for solid organs that include the sensing of growth factor concentrations and replenishment through stem cell differentiation (1, 2). However, how circulating cell populations achieve and maintain their appropriate cell numbers is unclear. For example, although peripheral naïve T cells are long lived (several months in mice and up to decades in humans) and are maintained at near constant numbers in adults (3-7), the underlying mechanisms remain unknown. Previous work has implicated both major histocompatibility complex:T cell receptor (TCR) interaction and interleukin signaling in peripheral T cell survival (8), which are important for T cell development and selection in the thymus (9), differentiation to memory T cells in the periphery upon antigenic stimulation (10) and T cell expansion (11). However, peripheral T cell survival can occur independently of both pMHC:TCR and interleukin signaling (12-14) and therefore they do not define T cell population densities. T cells have been proposed to occupy distinct ‘spaces’ (also termed ‘niches’) (15, 16), but any molecular or cell biological understanding of ‘space’ and ‘niche’ is currently lacking.

One protein that has been implicated specifically in the establishment and maintenance of appropriate peripheral T cell populations is coronin 1 (also known as P57 or TACO, for tryptophan aspartate containing coat protein), a member of the conserved WD repeat containing protein family (17-22). Coronin 1 is predominantly expressed in leukocytes and to a lesser degree in neurons (17, 22-24). Coronin 1 associates with phospholipase C (PLC) (25) and modulates intracellular trafficking in a Ca<sup>2+</sup> and cAMP-dependent manner (17, 26-28). Furthermore, coronin 1 has been suggested to be involved in the regulation of F-actin dynamics (19, 21), although F-actin-dependent leukocyte functions are not affected by

deletion of coronin 1 (26, 29). Coronin 1 is one of the most abundant proteins in T cells, and mice and humans deficient in coronin 1 have substantially reduced (up to 90% less) peripheral T cells despite normal T cell differentiation, selection, and export from the thymus as well as normal TCR and interleukin-7 signaling (14, 19, 20, 30, 31). However, the mechanism via which coronin 1 controls peripheral naive T cell population size is unclear.

Here, we report a coronin-dependent pathway controlling cell population size. We found that upon increases in cell density, the levels of coronin 1 increased further to ensure cell viability at elevated cell densities by promoting pro-survival  $Ca^{2+}$  signaling and inhibiting cell death. Inhibition of cell death signaling by coronin 1 occurred through dampening of surface expression of the cell adhesion molecules lymphocyte function-associated antigen 1 (LFA-1) and its ligand intercellular adhesion molecule 1 (ICAM1) to prevent premature induction of cell death. At or beyond appropriate cell densities, coronin 1 expression leveled off, thereby resulting in an increase in cell surface expression of LFA-1/ICAM1 that in turn activated apoptosis. Finally, we provide evidence for a role of coronin A, the coronin 1 homologue expressed in amoeba, in cell population size control involving its regulation of the expression of cell-to-cell adhesion signaling molecules. Together, the data show that T cells and amoebae intrinsically sense and regulate their population densities and suggest that coronin family members may have evolved to perform this evolutionary conserved cell population size control role by regulating the expression of kin-to-kin adhesion molecules.

## Results

### *Cell density-dependent increase of coronin 1 expression allows T cell population expansion*

The establishment of the circulating pool of T cells critically depends on coronin 1 to prevent caspase-mediated apoptosis; however, coronin 1 is dispensable for T cell production in the bone marrow and selection in the thymus (14, 18, 30). Consistent with a crucial role for coronin 1 in maintaining sustained cell population numbers in peripheral lymphoid organs, its expression was significantly up-regulated at the stage just prior to thymic exit into secondary lymphoid organs (Fig. 1A and fig. S1A). Furthermore, although already among the 2-5% most abundant proteins expressed in T cells (32, 33), coronin 1 protein levels were significantly elevated in T cells in the high-density environment of lymph nodes (~70% T cells) compared to in those in the low-density environment of the spleen (30% of T cells) (Fig. 1, B and C). The density-dependent increase of coronin 1 was T cell-intrinsic, because quantitative mass spectrometry analysis showed a three- to four-fold increase in coronin 1 expression (becoming the 11<sup>th</sup> most abundant protein) in Jurkat T cell cultures grown to high density as compared to being ranked 121 (out of 6779 detected proteins) in those grown in low densities (Fig. 1D and Data File S1). T cells expanded in vitro as long as coronin 1 levels increased (Fig. 1E and fig. S1B), after which cells stopped expanding and instead underwent cycles of caspase-mediated apoptosis (Fig. 1E,F). At low density cell populations, coronin 1 was fully dispensable for cell viability and population growth. However, *Cor1*<sup>-/-</sup> cell populations stopped expanding and instead underwent cycles of apoptosis at far lower cell densities (~1.5x10<sup>6</sup> cells/ml) and thus reached lower cell population levels than WT cell populations (Fig. 1G,H, fig. S1C-G and Data Files S2 and S3). The lower survival threshold of cells lacking coronin 1 was not due to enhanced metabolic activity (fig. S1H), nutrient depletion or release of cell death-promoting factors, because culturing WT cells in conditioned medium from coronin 1-deficient cells and vice versa did not alter cell growth

and survival significantly (Fig. 1I,J). Co-cultures of different ratios of WT and coronin 1-deficient cells resulted in density-dependent loss of coronin 1-deficient cells and increased representation of WT cells (Fig. 1K,L). Together, these results support the existence of a T cell-intrinsic coronin 1-dependent mechanism that regulates cell population size by setting the threshold at which T cells initiate cell death to regulate cell numbers within the population.

*Coronin 1 regulates T cell population size by modulating density-dependent adhesion-mediated cell death*

To determine the mechanism underlying coronin 1-dependent control of T cell population sizes, we analyzed a previously published RNAseq dataset (31), which revealed significant deregulation of virtually all cell-to-cell adhesion pathways in viable coronin 1-deficient mouse T cells (Fig. 2A-C and Data File S4). One of the differentially expressed genes encoded intercellular adhesion molecule 1 (ICAM1), a ligand for the heterodimeric lymphocyte function-associated antigen 1 (LFA-1), which consists of an integrin alpha L (ITGAL) and an integrin beta 2 (ITGB2) subunit (34). Both ICAM1 and LFA-1 were significantly and specifically increased at the cell surface of both peripheral mouse mature naive T cells and Jurkat T cells lacking coronin 1 (Fig. 2D and fig. S2A,B). The upregulation of cell surface LFA-1 and ICAM1 upon coronin 1 deletion occurred in low density cultures when apoptosis was not initiated (fig. S2A) and was therefore not a consequence of cell death. Instead, this finding suggested that coronin 1 reduced the surface expression of ICAM1 and LFA-1.

Observation of cell population dynamics by long-term imaging showed that upon cell density increase, cells lacking coronin 1 formed large multicellular aggregates in both human and murine T cell cultures (Fig. 2C,E and fig. S2C) and showed increased cell death as shown by propidium iodide staining (Fig. 2E and Movies S1 and S2). Furthermore, aggregates of apoptotic cells were detected by TUNEL assay in the spleens and lymph nodes from coronin 1-deficient mice, but not those from WT mice (Fig. 2F and fig. S2E). However, no notable differences were observed in the thymus (fig. S2D,E). Moreover, and consistent with an essential role for coronin 1 in controlling the size of the peripheral T cell population, but not in thymic development and selection (30), LFA-1 and ICAM1 surface expression were similar between WT and coronin 1-deficient mouse thymocytes at all stages of thymic development (fig. S2F). These data suggest that coronin 1 inhibits adhesion-mediated cell death signaling possibly by limiting the cell surface expression of LFA-1 and ICAM1, thereby enabling cells to expand to their appropriate cell population densities.

We next sought to directly determine whether the coronin 1-regulated interaction between LFA-1 and ICAM1 served to sense and modulate cell population density. Function blocking antibodies directed against ICAM1 or LFA-1 reduced (with ICAM1 and ITGAL antibodies) or prevented (with ITGB2 antibodies) cell aggregation and restored cell viability in coronin 1-deficient T cells, thereby enabling cell numbers to expand to near WT levels (Fig. 2G,H and fig. S3A,B). The ability of both ICAM1 and LFA-1 function blocking antibodies to prevent cell death (Fig. 2H and fig. S3C) suggests that the observed loss of viability did not result from integrin signaling in the absence of its ligands (35, 36). Furthermore, these data showed that integrin ligation-induced signaling, which has thus far been exclusively associated with pro-survival signaling (37, 38), can be coupled to the induction of cell death through density-dependent LFA-1- and ICAM1-mediated signaling.

We next investigated how coronin 1-regulated density-dependent LFA-1- and ICAM1-mediated cell death at elevated cell population sizes was induced. When mouse T cells were seeded at increasing densities, cells lacking coronin 1 underwent cell density-dependent cell death, whereas the viability of coronin 1-expressing WT cells remained comparable at both densities (fig. S4A). Moreover, CD4<sup>+</sup> T cells from the peripheral blood of an individual with a T cell deficiency due to a homozygous destabilizing V134M mutation in coronin 1 (27, 39) showed elevated surface abundance of both ICAM1 and LFA-1 (Fig. 3A and fig. S4B). Finally, we analyzed the consequences of in vivo blockade of LFA-1 using adoptive transfer in mice to avoid confounding effects on T cell generation given the essential roles for both LFA-1 and ICAM1 in thymocyte development (40). We assessed T cell population frequency and size at day 2 (in the blood) and day 4 (from pooled lymphoid organs that included blood, spleen and lymph nodes; Fig. 3B) to separate the reported potential short-term effects of blocking LFA-1 on T cell homing to lymph nodes (41) from long-term compensation by  $\alpha_4$  integrin receptors (42). Also, because LFA-1 is implicated in both homing and retention of lymphocytes within lymph nodes (43), lymphoid organs were pooled to separate survival advantages over migration or retention within the different lymphoid organs. Blocking LFA-1 resulted in significantly elevated T cell numbers in blood and lymphoid organs compared to the controls (Fig. 3C,D and fig. S4C,D). Similarly, T cell numbers were significantly increased by LFA-1 blockade for adoptive transfer of coronin 1-deficient T cells (fig. S4E). Together, these data suggest that coronin 1-regulated cell density-dependent integrin-mediated signaling is crucial for maintenance of the appropriate T cell population size in vivo.

*Coronin 1 moderates kin-to-kin cell density signaling by promoting LFA-1 internalization*

The data above suggest that coronin 1 suppressed the surface expression of LFA-1 and ICAM1 to limit premature cell death at low density. To directly assess a role for coronin 1-dependent control of cell population sizes through the regulation of integrin surface expression and cell death, WT T cells were cultured at low density to maintain low coronin 1 and surface ITGB2 levels (Fig. 3E, fig. S4F and fig. S5A-C), re-seeded at increasing densities and examined 24 and 48 hours later (we refer to this as a ‘density shock’ experiment). Within this short time, cells did not increase coronin 1 expression (fig. S5D), but showed significant density-dependent increase in surface ITGB2 levels (up to ~5-fold increase) and loss of viability (up to ~80%) with increasing density (Fig. 3F,G). Similarly, ITGB2 levels increased and cell viability decreased in T cells isolated from human peripheral blood mononuclear cells subjected to density shock (fig. S5G). Conversely, when cells were cultured to high densities, which significantly increased coronin 1 abundance, prior to re-seeding at increasing densities (fig. S5B), ITGB2 cell surface expression was comparatively repressed and cell viability was significantly enhanced (Fig. 3F,G and fig. S5D-F). Moreover, increased cell surface integrin levels preceded cell death (Fig. 3H), suggesting that density-dependent cell death was a consequence of increased ITGB2 surface expression.

We next assessed the role for coronin 1 in LFA-1 surface expression. First, we found by flow cytometry that although the total cellular levels of ITGB2 were comparable (fig. S6A), WT Jurkat T cells presented significantly less ITGB2 molecules at the cell surface compared to coronin 1-deficient cells (fig. S2A). This finding was corroborated by the significant ITGB2 cytoplasmic localization in WT cells compared to the largely peripheral localization in coronin 1-deficient cells as detected by immunofluorescent labelling (Fig. 3I and fig. S6B-D). Because of the roles for coronin 1 in endosomal traffic in macrophages and neurons (17, 28, 44) and its reported interaction with the cytoplasmic tail of ITGB2 (45), we analyzed whether

coronin 1 regulates cell surface integrin levels through intracellular retention. First, shifting WT Jurkat cells maintained at low density (and hence expressing relatively low coronin 1 levels) to high density resulted in a significant ( $>10$ -fold) increase in the surface/total ITGB2 ratio (fig. S6E). This ratio decreased  $\sim 3$ -fold after 48 hours, when the density had dropped again as a result of cell death (fig. S6E) suggesting that the relatively limited levels of coronin 1 protein were unable to prevent the cell surface exposure of ITGB2. Consistent with a role for coronin 1 in retaining ITGB2 intracellularly, ITGB2 was more rapidly internalized from the cell surface of WT Jurkat T cells compared to coronin 1-deficient cells (Fig. 3J).

*Coronin 1 couples the regulation of cell density-dependent LFA-1-mediated signaling to pro-survival  $Ca^{2+}$  mobilization.*

We next investigated a potential link between the reported role for coronin 1 in pro-survival signaling through  $Ca^{2+}$  mobilization downstream of PLC (18) and coronin 1-regulated density-dependent LFA1 function. First, analysis of RNAseq data (31) showed significant deregulation of genes involved in  $Ca^{2+}$  signaling (fig. S7A,C) and in activation of phospholipase C (fig. S7B,D) in coronin 1-deficient mouse T cells, consistent with previous work showing a role for coronin 1 in these pathways (18, 20, 26, 46). In addition, we found that in high-density cultures, store-released  $Ca^{2+}$  levels were reduced in coronin 1-deficient Jurkat T cells compared to WT cells, a difference that was not observed in low-density cultures (Fig. 4A). Moreover, and consistent with the role of adequate cytosolic  $Ca^{2+}$  levels in promoting cellular survival (47, 48), pharmacological elevation of  $Ca^{2+}$  in cells lacking coronin 1 significantly increased cell viability (Fig. 4B). Furthermore, when cultured to high densities in the presence of function blocking LFA-1 antibodies, the defect in  $Ca^{2+}$

mobilization was reversed in cells lacking coronin 1 (Fig. 4C), suggesting that the  $\text{Ca}^{2+}$  mobilization defect induced by coronin 1 deletion is associated with defective density-dependent regulation of LFA-1 function. These data therefore suggest that coronin 1 serves to maintain viability and pro-survival  $\text{Ca}^{2+}$  mobilization to counteract increased LFA-1/ICAM1-mediated signaling and the ensuing apoptosis until appropriate cell numbers are reached, thereby enabling the maintenance of proper cell population sizes.

#### *Coronins and adhesins play an evolutionary conserved role in cell population size control*

The above reported role for coronin 1 in regulating T cell density is intriguing given that coronin 1 is a close homologue of coronin A expressed in the slime mold *Dictyostelium discoideum* (22, 27, 49, 50). *D. discoideum* live as single cells that continuously sense their population density: When their cell density reaches a certain threshold amid limited food resources, instead of undergoing apoptosis, *D. discoideum* initiates a multicellular differentiation program to ensure their long-term survival (51). The finding that coronin 1 is required for kin-to-kin density sensing and maintenance of T cell population size prompted us to analyze the population dynamics of *D. discoideum* expressing or lacking coronin A under nutrient-rich conditions. When seeded at the same initial cell density, cells lacking coronin A were unable to reach the population density attained by WT cells (Fig. 5A). Similarly to T cells (Fig. 1D), relative coronin A abundance increased in a density-dependent fashion in *Dictyostelium* (fig. S8A,B). *D. discoideum* lacking coronin A and sampled at low cell density had a proteomic profile that resembled that of WT cells at high density (Fig. 5B-F and Data File S5). Functional annotation of the differentially expressed proteins revealed “cell-cell adhesion” as the most significantly enriched process (Fig. 5C). Notably, the four discoidins (Fig. 5D,E,F), which are major cell-cell adhesion molecules in *Dictyostelium* (52-55) and

whose expression is cell density-dependent, becoming up-regulated in WT *D. discoideum* at high cell density (56), were already significantly up-regulated in *corA*<sup>-</sup> cells at much lower densities (fig. S8C,D). Together, these data suggest that the absence of coronin A phenocopies a state of high cell density that limits cell population expansion and that coronin A is required to set the threshold for cell population size, similar to the role of coronin 1 in T cells (Fig. 6). Because *Dictyostelium* lacking coronin do not undergo cell death yet cannot reach WT cell densities, these data also suggest that the primary role of coronin is to enable cells to coordinate their population density and, rather than just supporting cell survival, coronin is required for cells to reach and maintain appropriate cell population sizes.

## **Discussion**

Our results provide evidence for the existence of an evolutionarily-conserved coronin-regulated pathway controlling cell population sizes. Our data suggested that kin-to-kin cell-cell interaction and the frequency and strength of their ensuing signal may serve to inform the cells of their relative population size and shape the population behavior, such that coronin 1 enables integration of cellular responses and population size. We showed that coronin 1 regulated cell population size through its dual role in suppressing cell surface expression of LFA-1 and ICAM1 and promoting pro-survival signaling through Ca<sup>2+</sup> mobilization upon increases in cell population density. This dual role would prevent premature kin-to-kin perception during cell population increase and the consequent premature initiation of population control including through the induction of cell death, allowing cell populations to reach and maintain appropriate cell density. The threshold at which LFA-1/ICAM1 ligation-initiated cell death was set by the amount of available coronin 1. Moreover, coronin 1 levels

correlated with T cell densities, with increased levels in T cells residing within the high T cell density environment of the lymph nodes compared to those in the relatively lower T cell density environment of the spleen. Although already one of the most abundant proteins in T cells, far higher coronin 1 levels (up to a four-fold increase) were required to sustain cell viability at increased cell density by promoting ICAM1/LFA-1 internalization and maintaining pro-survival signaling such as through  $Ca^{2+}$  mobilization. This is interesting given that this capacity of coronin 1 to regulate cell population size by coupling ITGB2 internalization and  $Ca^{2+}$ -mobilization mimics its role in regulating the intracellular survival of pathogenic mycobacteria within macrophages (26). It should also be noted that LFA-1/ICAM1 ligation has thus far been associated with pro-survival signaling, whereas the here-observed death pathway mediated through LFA-1/ICAM1 interaction may involve hitherto undefined signaling intermediates, possibly including the engagement of other co-receptors. Although LFA-1 is required for homotypic cell-cell adhesion, it might not necessarily be the molecule that initiates the apoptotic process. Together, the data support a T cell-intrinsic, coronin 1-dependent mechanism for sensing and controlling cell population.

It is important to note that the coronin 1-dependent regulation of cell density operated in naive and non-stimulated cells. In fact, because T cell differentiation, cytokine-mediated stimulation, and activation through the T cell-receptor are not perturbed by the absence of coronin 1 (14), coronin-dependent control of cell population size may have evolved to regulate the long-term maintenance of multicellular populations at their appropriate density, rather than acting to differentiate and/or activate cells. How coronin 1-dependent cell population density regulation may operate after T cell stimulation and proliferation during immune responses and memory T cells formation when cell numbers need to return to normal levels remains to be analyzed.

We inferred that the role for coronins and adhesion molecules in controlling cell population size may have its origin at the single cell eukaryote stage, consistent with the roles for coronin 1 and coronin A in regulating these processes in vertebrates and *Dictyostelium*, respectively. Moreover, both coronins and integrins may have evolved during the unicellular-to-multicellular transition (57, 58), when a kin-to-kin density sensing pathway would have enabled the integration of environmental cues with multicellular dynamics while maintaining genetic diversity. Furthermore, in humans, both genes encoding coronin 1 and the LFA-1 subunit ITGAL are located on the chromosome 16p11.2 locus, suggesting long-term coevolution, co-regulation, or both (59, 60).

Our results suggest that cells perceive their population density through coronin-regulated cell-cell interactions and adjust their cellular components and population behavior accordingly. Further studies should include identifying how cell-cell signal strength thresholds are set, the signaling intermediates involved in the control of cell population sizes, and the potential transcriptional adjustments to gene expression.

The evolutionarily conserved coronin- and adhesion molecule-dependent mechanism regulating cell density described here now allows a molecular definition of what has thus far been termed the ‘space’ occupied by immune cell populations. Also, this pathway may be relevant when the immune system needs to be re-established, such as after hematopoietic stem cell transplantation (61). Furthermore, given the current surge in T cell-mediated therapies, during which it is imperative to control cell density and longevity to allow effectiveness while avoiding uncontrolled growth (62), detailed knowledge of the molecules involved in cell density sensing and maintenance of appropriate cell population sizes may

lead to more effective approaches. Finally, whether other coronin family members, several of which have been implicated in the control of cell numbers (22, 63), are similarly involved in density sensing and cell population size control remains an interesting question for the future.

## Materials and Methods

### *Cells*

Jurkat cells (ECACC, Sigma 88042803) were grown in RPMI-1640 (Sigma, #R8758 or Gibco, #31870-025) supplemented with 10% FBS (PAA or Gibco), 2 mM L-glutamine (Gibco) and containing 100 U/ml penicillin and 0.1 mg/ml streptomycin (Sigma, #4333).

Cells were incubated in a 37° C humidified incubator with a 5% CO<sub>2</sub>. *Dictyostelium discoideum* wild type, *corA*- and complemented strains have been described before (50) and were grown in shaking culture at 160 RPM and 22°C in HL5 medium.

### *Mice*

Coronin 1-deficient mice (The Jackson Laboratory stock no. 030203) were backcrossed to C57/BL6 and used from backcross 8 or backcross 10 as described before (18). *Rag2*<sup>-/-</sup> (64) mice were obtained from Prof. Ed Palmer (Basel, Switzerland). Cohorts were age (6-16 weeks) and sex matched and both male and female mice were used for the studies. Animal experiments were performed following the cantonal veterinary rules and regulation at the animal facility of the Biozentrum, University of Basel.

### *Human Blood Specimens*

Human PBMCs were isolated from healthy volunteers through the Blutspendezentrum, University Hospital Basel and from the V134M mutated human subject (male, ~22 years old) described earlier (39) using a Histopaque 1077 (Sigma Aldrich, #10771) column following the manufacturer's protocol.

### *Primary Culture*

Isolated mouse T cells and human PBMCs were cultured in RPMI-1640 (Sigma, #R8758 or Gibco, #31870-025) supplemented with 10% FBS (PAA or Gibco), 2 mM L-glutamine (Life Technologies, #25030), 1 mM sodium pyruvate (Sigma, #S8636), non-essential amino acids (Sigma, #M7145), 10  $\mu$ M 2-mercaptoethanol (Sigma, #M7522) and 100 U/ml penicillin and 0.1 mg/ml streptomycin (Sigma, #4333). Cells were incubated in a 37° C humidified incubator in a 5% CO<sub>2</sub> atmosphere.

### *Reagents*

Antibodies were from the following sources. Rabbit anti-coronin 1 antibody (serum 1002) has been described before (17). Mouse anti-coronin 1 was from Abnova (cat# H00011151-M01) and rabbit anti-coronin 1 was from Abcam (Abcam #: ab123574). Antibodies against coronin A were described before (50). Flow cytometry antibodies used were from Biolegend and Becton Dickinson. Anti-ITGAL and anti-ICAM1 were from Santa Cruz Biotechnology (#sc-374172 and #sc-8439, respectively). Functional blocking antibodies against ICAM1 (clone P2A4, developed by E. A. Wayner and G. Vercellotti) and LFA-1 (ITGAL clone TS1/22.1.1.13.3 and M17/4.4.11.9; ITGB2 clone H52, developed by Tim Springer) were obtained from the Developmental Studies Hybridoma Bank. Actin antibody (MAB1501) was from Merck Millipore. Histopaque 1077 was from Sigma.

### *Deletion of the coronin 1 gene in Jurkat T cells by CRISPR/Cas9 Genome Editing*

pSpCas9(BB)-2A-GFP (PX458) was a gift from Feng Zhang (Addgene plasmid # 48138). A 20-nucleotide sequence targeting the third exon of human coronin 1 followed by a protospacer adjacent motif (PAM) from *Streptococcus pyogenes* [CAGGGGCTCACCTTGCCAG(GGG)] was selected using publicly available tools for the

least number of potential off-target sites. The sequence was cloned into PX458 as previously described (65). Jurkat T cells ( $1 \times 10^6$ ) were transfected with 7.5  $\mu$ g of pX458-sgRNA plasmid in a 6-well tissue culture plate using the Xfect™ Transfection Reagent (Takara Bio, Cat# 631318) according to the manufacturer's protocol. GFP-expressing cells were sorted 48 h after electroporation and enriched, then sorted again after a week and assessed for editing (loss of coronin 1 expression). After confirming the occurrence of edited cells, we sorted the cells into 20, 10, 5, and 1 cell per well into 96-well tissue culture plates, expanded the clones, and screened for coronin 1 knockout clones by flow cytometric and microscopic analysis of intracellularly-stained cells. More than 20 coronin 1-deficient clones were isolated and showed a similar phenotype in culture (Data File S1). Three clones were randomly selected and the absence of coronin 1 expression was further confirmed by immunoblotting and genotyping using the Inference of Crispr Edited (ICE)-based webtool (<https://ice.synthego.com/#/>). All coronin 1-deficient clones possessed the same indel. The clones shown are coronin 1-deficient Jurkat clone 20-23 (*Cor1*<sup>-/-</sup> cl.1) and 5-B11 (*Cor1*<sup>-/-</sup> cl.2). As a control, we used one of the cloned cells that expressed WT levels of coronin 1 (clone 5-A3, WT cl.1).

#### *Generation of complemented Jurkat T cell clone*

The pLenti-GIII-EF1a-hCORO1A plasmid, which was obtained from Abmgood (Richmond, Canada), had the EF1a promoter driving human coronin 1 coding DNA sequence (CDS). This plasmid did not encode a stop codon, and therefore we introduced KpnI-ClaI restriction sites through the NheI site using the primer pair CTAGCGGGTACCAATCGAT and CTAGATCGATTGGTACCCG). Subsequently, the region harboring the CDS was digested away with KpnI-XbaI and replaced with the full length human coronin 1 CDS flanked with KpnI-XbaI restriction sites to generate pLenti-GIII-EF1a-hCORO1A expressing the full

length human CORO1A driven by the EF1a promoter. Lentiviral particles were packaged in HEK293T cells and used for Jurkat cell transduction. Transduced cells were selected by puromycin and showed substantial variability of coronin 1 expression as determined by flow cytometry analysis of fluorescently labelled cells. Clonally expanded cells with the highest expression levels of coronin 1 (although below WT levels) were selected for further studies.

#### *Cell viability analysis*

The numbers and viability of Jurkat and mouse T cells were routinely analyzed using Trypan blue exclusion using a standard Neubauer chamber. Any aggregates, including those induced upon coronin 1 deletion, were easily disaggregated by gentle repeated pipetting as used in this procedure.

#### *Isolation of viable cells for protein and RNA Isolation*

To separate viable from non-viable cells, Jurkat T cells used for protein and RNA isolation were first passed through a Histopaque 1077 (Sigma Aldrich, #10771) column following the manufacturer's protocol. Only viable cells were collected for subsequent analysis.

#### *Cell lysis and immunoblotting*

Viable cells were lysed in RIPA (50 mM Tris-HCl pH7.4, 150 mM NaCl, 1% NP-40, 0.5% sodium deoxycholate (NaDOC), 0.1% SDS, 1 mM EDTA) buffer containing halt protease and phosphatase inhibitor cocktail (Thermo Scientific, Cat# 1861284) at 4°C as described (27). Proteins (20 µg, as determined by the BCA assay, Pierce) were separated on 10% sodium dodecyl sulfate polyacrylamide gel electrophoresis (SDS-PAGE) gels and transferred onto nitrocellulose membranes with semi-dry transfer systems (BioRad, Hercules, CA, USA). The membranes were stained with Ponceau red protein stain for 10 min, rinsed with ddH<sub>2</sub>O

and scanned with a CanoScan 9000F Mark II scanner (Canon). The Ponceau red was washed off and the membrane blocked with 5% milk in PBS-Tween20 for 1 h at room temperature or overnight at 4 °C. The antibodies were diluted in 5% milk PBS-Tween20 (1:1000 for mouse anti-coronin 1, 1:1000 mouse ITGβ2 (H52), 1:200 mouse anti-ITGAL (Santa Cruz Biotechnology #sc-374172), 1:200 mouse anti-ICAM1 (Santa Cruz Biotechnology #sc-8439) and 1:5000 for anti-actin). Primary antibody incubation was done either at room temperature for 2 h or overnight at 4 °C. After washing, membranes were incubated with horseradish peroxidase (HRP)-coupled secondary antibodies (Southern Biotech) (66). Membranes were developed using WesternBright Quantum HRP substrate (Advansta) and imaged using a Fusion FX7 (VILBER, Paris, France).

#### *Flow cytometry*

For cell surface staining, equal numbers of cells (typically  $0.4-1 \times 10^6$  cells) were incubated in 96-well U-bottom plates with the indicated antibody combinations in FACS buffer (phosphate buffered saline supplemented with 2% FCS and 2 mM EDTA) for 30 min on ice. Antibodies were used at 1:100. Live/Dead Marker was used at 1:1000. After staining, cells were pelleted (5 min at 4°C, 450xg), resuspended in 200 µl FACS buffer, transferred to polystyrene tubes, and analyzed within 2 hours using a BD LSR Fortessa Analyzer or BD FACS CantoII Analyzer. For intracellular staining, equal numbers of cells (typically  $0.4-1 \times 10^6$  cells) were transferred in 96-well U-bottom plates, incubated on ice for 15 min with 1:1000 Live/Dead APC/Cy7 solution in PBS-Dulbecco (DPBS) buffer, harvested (4 min at 4 °C, 450xg), fixed with 4% PFA/DPBS (15 min at 4 °C), and incubated (15 min at 4 °C) with permeabilization buffer (PBS, 2% FCS, 10 mM EDTA, 0.1% saponin, 0.05% Na-azide). After permeabilization, cells were pelleted (5 min at 4°C, 450xg), resuspended in antibody diluted in permeabilization buffer, incubated for 30 min on ice, and incubated with 1:500

dilution of the Alexa Fluor-568 or -647 labelled secondary antibody in permeabilization buffer for 30 min on ice. Cells were washed and pelleted (5 min at 4°C, 450xg) and resuspended in 200 µL FACS buffer and transferred to polystyrene tubes and analyzed within 2 hours using a BD LSR Fortessa Analyzer or BD FACS CantoII Analyzer. Cell surface or intracellular staining data were analyzed using FlowJo software (Tree Star).

Apoptosis and necrosis was analyzed using the Abcam Apoptosis/Necrosis Detection Kit (blue, green, red) (Abcam, Cat#ab176749) according to the manufacturer's protocol. Caspase 3/7 activity was analyzed using the ImmunoChemistry Technologies' Magic Red Caspase-3/7 Assay Kit (ImmunoChemistry, Cat# 936) according to the manufacturer's protocol. For both apoptosis/necrosis and Caspase 3/7 assays, the BD LSR Fortessa Analyzer was used.

#### *Immunofluorescence analysis*

Cells were seeded on poly-L-lysine-coated 10-well Teflon coated slide (Thermo) for 1h at 37°C with 5% CO<sub>2</sub>. For colocalization analysis, cells were transferred from culture onto ice and allowed to attach on poly-L-lysine-coated slide at 4 °C. Attached cells were fixed with ice-cold 100% methanol for 5 min and blocked with 2% FBS, 3% BSA in PBS. Cells were incubated with primary antibodies (1:500 dilution of rabbit anti-coronin 1 (1002) or mouse anti-ITGB2 (H52) or both) in a solution of PBS containing 1.2% FBS/1.8% BSA/0.02% Tween 20 for 30 min at room temperature or overnight at 4 °C. Next, cells were incubated with 1:500 dilution of Alexa Fluor 568 donkey anti-rabbit and/or Alexa Fluor 488 donkey anti-mouse labelled secondary antibody (Invitrogen #A-10042 and #A-21202) at room temperature for 1h. Stained samples were mounted with Fluoroshield Mounting Medium (Sigma #F6182) and slides were visualized using a 60x oil immersion objective on a Nikon Ti2E microscope.

### *Live cell imaging*

For live cell imaging, cell cultures supplemented with propidium iodide (0.5 µg/ml) with or without function blocking antibody in 96 well plates (Falcon® 96-well Black/Clear Flat Bottom TC-treated Imaging Microplate with Lid, Cat#: 353219) were imaged on a Nikon Ti2E microscope with a 37 °C / 5% CO<sub>2</sub> incubator (Life Imaging Services GmbH, Basel, Switzerland).

### *Scanning Electron Microscopy*

Cells were grown on round coverslips (12 mm) that had been cleaned with ethanol and coated with poly-L-lysine. Cells were fixed with 2.5% glutaraldehyde in PBS and dehydrated in steps of 15 minutes in 30, 50, 70, 90, 100% (2x) ethanol. This procedure was followed by critical point drying (CPD, (67)). The dried samples were mounted on SEM stubs and sputtered with a 20nm layer of gold and analyzed using a Phillips XL 30 ESEM.

### *Lymphoid organ analysis*

To obtain mouse T cells, mice were euthanized with CO<sub>2</sub> and blood was sampled by cardiac puncture. The spleen, lymph nodes and thymus were harvested in ice cold Dulbecco's PBS containing 2% FBS and smashed through a gridded mesh (steel/nylon (Sefar AG)). Debris was removed by a quick spin (70xg, 3 sec). Blood and spleen cells were treated with ammonium-chloride-potassium (ACK) buffer (155mM NH<sub>4</sub>Cl, 10mM KHCO<sub>2</sub>, 1mM EDTA, pH 7.4) to remove red blood cells. Cells were counted and stained in FACS buffer (PBS, 2% FCS, 5mM EDTA) with the appropriate antibodies as indicated in the figure panels or described (30, 31). After antibody incubation, cells were washed twice with the same buffer and resuspended in 200 µl of FACS buffer. Fluorescence was measured using a BD LSR

Fortessa Analyzer or BD FACS CantoII Analyzer. Results were analyzed using FlowJo software (Tree Star).

For the ex vivo analysis of T cell survival, total splenic T cell was isolated using the EasySep Mouse T Cell Isolation Kit (Stemcell Technologies, Cat#: 19851) according to the manufacturer's instruction and naïve CD4 T cells were purified as described (30). Purified cells were cultured for the indicated times in RPMI medium supplemented with 10% fetal bovine serum, 1 mM sodium pyruvate, 2mM L-glutamine, non-essential amino acids (Sigma M7145), 50 µM beta-mercaptoethanol and 10 U/mL penicillin/streptomycin, with or without 20 ng/mL interleukin-7 (Biolegend cat#: 577802) and with or without purified anti-mouse ITGAL (M17/4.4.11.9). Cell viability was analyzed by Neubauer chamber counting or flow cytometry analysis of DAPI or Live/Dead APC/Cy7 staining (Invitrogen Cat# L10119). For naïve CD4 T cells, the live cell counts were analyzed by gating on live CD3<sup>+</sup>CD4<sup>+</sup>CD62L<sup>+</sup>CD44<sup>-</sup> cells per each sample.

#### *Histopathological analysis of lymphoid organs*

To analyze the thymus, spleen and lymph nodes, mice were sacrificed in a carbon dioxide chamber. Organs were dissected and isolated, fixed in 4% formalin overnight for 24 h, washed with ddH<sub>2</sub>O, embedded in paraffin, and sectioned. TUNEL staining was performed using ThermoFisher's Click-iT™ Plus TUNEL assay for in situ apoptosis detection with Alexa Fluor™ 647 dye (Cat#: C10619) following the manufacturer's protocol.

#### *Metabolic activity*

Metabolic activity was analyzed using Alamar blue (Sigma-Adrich, R7017-1G, 0.125 mg/mL) following the manufacturer's protocol. In brief, cells were cultured in a 96-well plate at the indicated densities and incubated with resazurin solution (10%, vol/vol, resazurin

sodium salt, 0.125 mg/mL, H<sub>2</sub>O) for 4 h at 37 °C. Fluorescence was measured at 540/588 nm using a microplate reader (Synergy H4, BioTek Instruments).

#### *Differential expression analysis*

Gene expression datasets obtained from WT or coronin 1-deficient conventional T cells (CD4<sup>+</sup>CD25<sup>-</sup>) were used (31). Differential expression analysis was conducted using DESeq2 modeling genotype (WT compared to Coro1A knock-out) with a cut-off of adjusted p-values < 0.01 and log<sub>2</sub> fold-change ≥ 1 (68-71). Statistically significant enrichment of Reactome pathway (72) annotation terms was assessed using ClusterProfiler (69).

#### *Integrin internalization assay*

ITGB2 internalization was performed essentially as described (73). Briefly, cells maintained in culture at less than 10<sup>6</sup> cells/mL were harvested, washed with D-PBS (Sigma, #10771), and washed twice with antibody staining and endocytosis medium (RPMI buffered with 20 mM HEPES, pH 7.4). Cell surface integrins were labelled with Alexa-Fluor 647 conjugated antibody to ITGB2 (clone CBR LFA-1/2, BioLegend, #366312) in antibody staining and endocytosis medium for 30 minutes at 4°C. Cells were washed twice with antibody staining and endocytosis medium and sampled before the start of internalization (start sample). The remaining cells were re-suspended in antibody staining and endocytosis medium prewarmed to 37 °C and incubated at 37 °C to allow endocytosis to occur for various intervals (15, 30, 45, 60, 75 or 90 minutes). Residual surface bound antibody was removed by washing the cells twice (2 minutes/wash) with antibody stripping buffer (50 mM glycine, 150 mM NaCl, pH 2.5) at 4°C with gentle agitation. Cells were washed with D-PBS and resuspended in FACS buffer (1x PBS, 2% FCS, 10mM EDTA, 0.05% Na-azide) containing 1 ug/mL 4',6-diamidino-2-phenylindole (DAPI) to distinguish between viable and dead cells.

Measurements were performed with BD LSR Fortessa, and data were analyzed using FlowJo software (FlowJo). The rate of ITGB2 internalization was determined as the percentage of the internalized signal to the signal from the start sample.

#### *Adoptive transfer with integrin function blocking*

*Rag2*<sup>-/-</sup> mice were administered D-PBS with or without 300 µg of purified rat anti-ITGAL (clone M17/4.4.11.9) antibody or the isotype control (rat anti-coronin 1 mAb clone GK3) on day -1 (D<sub>-1</sub>) intraperitoneally. The following day (D<sub>0</sub>), T cells were isolated from WT or coronin 1-deficient mice using the EasySep Mouse T Cell Isolation Kit (Stemcell Technologies, Cat#: 19851) and subjected to FACS-based purity checks. 10<sup>7</sup> T cells in D-PBS containing or not 300 µg M17/4.4.11.9 or GK3 were transferred into respectively pre-treated *Rag2*<sup>-/-</sup> mice by tail vein intravenous injection. Other control *Rag2*<sup>-/-</sup> mice received only DPBS with no cells. Two days later (D<sub>2</sub>), blood samples were collected to assess the T cell population. On the same day, another dose of D-PBS with or without 300 µg M17/4.4.11.9 or GK3 was administered intraperitoneally. On D<sub>4</sub>, animals were sacrificed, and the spleens, lymph nodes, blood and thymus sampled for total T cells present as described above. The contribution of T cell from the thymus was negligible (typically <0.005% of total T cells recovered). For animals that received cells, a total of four animals were treated with anti-LFA1 function blocking antibody (M17/4.4.11.9), three animals with the isotype control anti-coronin 1 (GK3, mouse monoclonal) and three animals with DPBS for each. In addition, control animals that received no cells were treated with DPBS only.

#### *Intracellular Ca<sup>2+</sup> Mobilization and Modulation*

Cells maintained in culture at low density (below 0.6×10<sup>6</sup> cells/mL) or at high density (above 2×10<sup>6</sup> cells/mL) were counted, harvested and normalized to equal cell numbers in their

respective supernatant. Cells were incubated with 2  $\mu\text{g/ml}$  of Indo-1 AM (ThermoFisher, Cat# I1223) for 45 min at 37 °C in the dark and gently agitated every 15 min in complete medium (including magnesium). After Indo-1 AM loading, cells were washed twice, resuspended in HBSS modified without  $\text{Ca}^{2+}$  and  $\text{Mg}^{2+}$ , allowed to equilibrate at 37 °C for 10-15 min, and supplemented with propidium iodide (0.5  $\mu\text{g/ml}$ ) to distinguish between live dead cells. To determine the intracellular  $\text{Ca}^{2+}$  levels, cells were analyzed by flow cytometry on a BD LSR Fortessa for 30 s to read the  $\text{Ca}^{2+}$ -bound (405 nm, reflecting the cytoplasmic  $\text{Ca}^{2+}$  levels) and  $\text{Ca}^{2+}$ -free (510 nm) Indo-1 signals and establish a baseline. PLC activation and intracellular  $\text{Ca}^{2+}$  flux was induced with 25  $\mu\text{M}$  m-3m3FBS or DMSO. Data were collected for an additional 300 s and analyzed using FlowJo software (Tree Star). To modulate intracellular  $\text{Ca}^{2+}$  levels and assess the effect on viability, cells were seeded at the indicated density with DMSO or the SERCA blocker thapsigargin at the indicated concentration, cultured for 120 h, and sampled for viability.

#### *Label-free quantitative proteomics analysis of Dictyostelium discoideum*

Cells were cultured as indicated in the figure panels. Cells ( $3 \times 10^6$ ) were pelleted, washed with ice cold DPBS, pelleted again and resuspended in lysis buffer (8 M urea, 0.1M ammonium bicarbonate, phosphatase inhibitors, 5 mM TCEP), and sonicated with a Bioruptor (10 cycles, 30 seconds on/off, Diagenode, Belgium). Proteins were alkylated with 10 mM chloroacetamide for 1 h at 37 °C. After diluting samples with 100 mM ammonium bicarbonate buffer to a final urea concentration of 1.6M, proteins were digested by incubation with sequencing-grade modified trypsin (1/50, w/w; Promega, Madison, Wisconsin) overnight at 37°C. After acidification using 5% TFA, peptides were desalted on C18 reversed-phase spin columns according to the manufacturer's instructions (Macrospin, Harvard Apparatus) and dried under vacuum. Peptides were dissolved in and adjusted to 0.5

$\mu\text{g}/\mu\text{l}$  with 0.1% formic acid and 1  $\mu\text{g}$  subjected to label-free quantification based LC-MS analysis as described previously (74). In brief, chromatographic separation of peptides was carried out using an EASY nano-LC 1000 system (Thermo Fisher Scientific) equipped with a heated RP-HPLC column (75  $\mu\text{m}$  x 37 cm) packed in-house with 1.9  $\mu\text{m}$  C18 resin (Reprosil-AQ Pur, Dr. Maisch). Aliquots of 1  $\mu\text{g}$  total peptides were analyzed per LC-MS/MS run using a linear gradient ranging from 95% solvent A (0.1% formic acid) and 5% solvent B (99.9% acetonitrile, 0.1% formic acid) to 30% solvent B over 120 minutes at a flow rate of 200 nl/min. Mass spectrometry analysis was performed on Q-Exactive HF mass spectrometer equipped with a nanoelectrospray ion source (both Thermo Fisher Scientific). Each MS1 scan was followed by high-collision-dissociation (HCD) of the 20 most abundant precursor ions with dynamic exclusion for 30 seconds. Total cycle time was approximately 1-2 sec. For MS1,  $3 \times 10^6$  ions were accumulated in the Orbitrap cell over a maximum time of 100 ms and scanned at a resolution of 120,000 FWHM (at 200 m/z). MS2 scans were acquired at a target setting of  $1 \times 10^5$  ions, accumulation time of 50 ms and a resolution of 15,000 FWHM (at 200 m/z). Singly charged ions and ions with unassigned charge state were excluded from triggering MS2 events. The normalized collision energy was set to 28%, the mass isolation window was set to 1.4 m/z and one microscan was acquired for each spectrum.

The acquired raw files were imported into the Progenesis QI software (v2.0, Nonlinear Dynamics Limited), which was used to extract peptide precursor ion intensities by applying the default parameters. The generated mgf files were searched with MASCOT against a decoy database containing normal and reverse sequences of the predicted SwissProt entries of *Dictyostelium discoideum* (www.ebi.ac.uk, release date 2017/10/09) and commonly observed contaminants (26,272 sequences in total) generated using the SequenceReverser tool from the MaxQuant software (Version 1.0.13.13). The search criteria were set as follows: full tryptic

specificity was required (cleavage after lysine or arginine residues, unless followed by proline); 3 missed cleavages were allowed; carbamidomethylation (C) was set as fixed modification; oxidation (M) and acetylation (Protein N-term) were applied as variable modifications; mass tolerance of 10 ppm (precursor) and 0.02 Da (fragments). The database search results were filtered using the ion score to set the false discovery rate (FDR) to 1% on the peptide and protein level, respectively, based on the number of reverse protein sequence hits in the datasets. The relative quantitative data obtained were normalized and statistically analyzed using our custom script as above (74).

#### *Tandem mass tags-based proteomics analysis of Jurkat T cells*

Cells were cultured as indicated in the figure panels and separated using Ficoll gradient centrifugation to separate live from dead cells using Histopaque-1077 (Sigma), following the manufacturer's protocol. Jurkat T cells ( $2 \times 10^6$ ) were pelleted and prepared as described above. Sample aliquots containing 10  $\mu$ g of peptides were dried and labeled with tandem mass isobaric tags (TMTpro 16-plex, Thermo Fisher Scientific) according to the manufacturer's instructions. Overall, 6 TMT experiments were carried out including 15 samples and one pooled sample containing aliquots of all 90 samples. After pooling the differentially TMT labeled peptide samples, peptides were again desalted on C18 reversed-phase spin columns according to the manufacturer's instructions (Macrospin, Harvard Apparatus) and dried under vacuum. TMT-labeled peptides were fractionated by high-pH reversed phase separation using a XBridge Peptide BEH C18 column (3,5  $\mu$ m, 130 Å, 1 mm x 150 mm, Waters) on an Agilent 1260 Infinity HPLC system. Peptides were loaded on column in buffer A (ammonium formate (20 mM, pH 10) in water) and eluted using a two-step linear gradient starting from 2% to 10% in 5 minutes and then to 50% (v/v) buffer B (90% acetonitrile / 10% ammonium formate (20 mM, pH 10) over 55 minutes at a flow rate

of 42  $\mu\text{l}/\text{min}$ . Elution of peptides was monitored with a UV detector (215 nm, 254 nm). A total of 36 fractions were collected, pooled into 12 fractions using a post-concatenation strategy as previously described (75), and dried under vacuum. Peptides (1  $\mu\text{g}$ ) were LC-MS analyzed as described previously (74). Chromatographic separation of peptides was carried out using an EASY nano-LC 1000 system (Thermo Fisher Scientific) equipped with a heated RP-HPLC column (75  $\mu\text{m}$  x 37 cm) packed in-house with 1.9  $\mu\text{m}$  C18 resin (Reprosil-AQ Pur, Dr. Maisch). Aliquots of 1  $\mu\text{g}$  total peptides were analyzed per LC-MS/MS run using a linear gradient ranging from 95% solvent A (0.15% formic acid in water) and 5% solvent B (80% acetonitrile, 19.9% water, 0.1% formic acid) to 30% solvent B over 70 minutes and to 45% solvent B over another 20 min. at a flow rate of 200  $\text{nl}/\text{min}$ . Mass spectrometry analysis was performed on Q-Exactive HF mass spectrometer equipped with a nanoelectrospray ion source (both Thermo Fisher Scientific). Each MS1 scan was followed by high-collision-dissociation of the 10 most abundant precursor ions with dynamic exclusion for 20 seconds. Total cycle time was approximately 1 s. For MS1, 3e6 ions were accumulated in the Orbitrap cell over a maximum time of 100 ms and scanned at a resolution of 120,000 FWHM (at 200  $\text{m}/\text{z}$ ). MS2 scans were acquired at a target setting of 1e5 ions, accumulation time of 100 ms and a resolution of 30,000 FWHM (at 200  $\text{m}/\text{z}$ ). Singly charged ions and ions with unassigned charge state were excluded from triggering MS2 events. The normalized collision energy was set to 30%; the mass isolation window was set to 1.1  $\text{m}/\text{z}$ ; and one microscan was acquired for each spectrum. The acquired raw files were searched against a protein database containing sequences of the predicted SwissProt entries of *Homo sapiens* ([www.ebi.ac.uk](http://www.ebi.ac.uk), release date 2019/03/21), and commonly observed contaminants (17,175 sequences in total) using the SpectroMine software (Biognosys, version 1.0.20235.13.16424) and the TMTPro default settings. In brief, the precursor ion tolerance was set to 10 ppm and fragment ion tolerance was set to 0.02 Da. The search criteria were set as follows: full tryptic specificity

was required (cleavage after lysine or arginine residues unless followed by proline), 3 missed cleavages were allowed, carbamidomethylation (C), TMTpro (K and peptide n-terminus) were set as fixed modification and oxidation (M) as a variable modification. The false identification rate was set to 1% by the software based on the number of decoy hits. Proteins that contained similar peptides and could not be differentiated based on MS/MS analysis alone were grouped to satisfy the principles of parsimony. Proteins sharing significant peptide evidence were grouped into clusters. The different TMT experiments were combined using the pool channel based internal reference scaling (IRS) approach described previously (76). In brief, a geometric means of pool channels from all TMT sets was calculated for each protein. For each TMT set, a protein specific scaling factor was calculated as ratio of geometric mean to the reference channel intensity. The IRS corrected protein intensities were then used for differential analysis using SafeQuant R script (v2.3, (74) with disabled normalization step. The analysis was based on empirical Bayes moderated t- statistics. Derived p-values were corrected for multiple testing using the Benjamini–Hochberg method.

#### *Quantification and Statistical analysis*

Statistical analyses were performed with GraphPad Prism Software (version 8) or Excel (Microsoft office). Gene ontology was performed using Panther (<http://www.pantherdb.org/panther/ontologies.jsp>). Comparisons between two groups were performed with the unpaired Student's *t*-test or the Mann-Whitney *U*-test (when the groups were independent and did not have a normal distribution). P values: \* P<0.05, \*\* P<0.01, \*\*\*P<0.001 and \*\*\*\*P<0.0001. Error bars normally show standard deviation unless otherwise indicated.

## Supplementary Materials

Figs. S1-S8.

Data Files S1-S5

Movies S1 and S2

## References and Notes

1. H. Gehart, H. Clevers, Tales from the crypt: new insights into intestinal stem cells. *Nat Rev Gastroenterol Hepatol* **16**, 19-34 (2019).
2. A. Sanchez Alvarado, S. Yamanaka, Rethinking differentiation: stem cells, regeneration, and plasticity. *Cell* **157**, 110-119 (2014).
3. I. den Braber *et al.*, Maintenance of peripheral naive T cells is sustained by thymus output in mice but not humans. *Immunity* **36**, 288-297 (2012).
4. N. Vrisekoop *et al.*, Sparse production but preferential incorporation of recently produced naive T cells in the human peripheral pool. *Proc Natl Acad Sci U S A* **105**, 6115-6120 (2008).
5. J. J. Thome *et al.*, Spatial map of human T cell compartmentalization and maintenance over decades of life. *Cell* **159**, 814-828 (2014).
6. J. A. M. Borghans, K. Tesselaar, R. J. de Boer, Current best estimates for the average lifespans of mouse and human leukocytes: reviewing two decades of deuterium-labeling experiments. *Immunological reviews* **285**, 233-248 (2018).
7. J. Sprent, D. F. Tough, Lymphocyte life-span and memory. *Science* **265**, 1395-1400 (1994).
8. J. Sprent, J. H. Cho, O. Boyman, C. D. Surh, T cell homeostasis. *Immunol Cell Biol* **86**, 312-319 (2008).
9. T. K. Starr, S. C. Jameson, K. A. Hogquist, Positive and negative selection of T cells. *Annu Rev Immunol* **21**, 139-176 (2003).
10. M. Polonsky *et al.*, Induction of CD4 T cell memory by local cellular collectivity. *Science* **360**, (2018).
11. J. Kirberg, A. Berns, H. von Boehmer, Peripheral T cell survival requires continual ligation of the T cell receptor to major histocompatibility complex-encoded molecules. *J Exp Med* **186**, 1269-1275 (1997).
12. P. Revy, M. Sospedra, B. Barbour, A. Trautmann, Functional antigen-independent synapses formed between T cells and dendritic cells. *Nat Immunol* **2**, 925-931 (2001).
13. J. R. Dorfman, R. N. Germain, MHC-dependent survival of naive T cells? A complicated answer to a simple question. *Microbes Infect* **4**, 547-554 (2002).
14. M. Mori *et al.*, Suppression of caspase 8 activity by a coronin 1-PI3Kdelta pathway promotes T cell survival independently of TCR and IL-7 signaling. *Science signaling* **14**, eabj0057 (2021).
15. K. Takada, S. C. Jameson, Naive T cell homeostasis: from awareness of space to a sense of place. *Nat. Rev. Immunol* **9**, 823-832 (2009).
16. B. Stockinger, T. Barthlott, G. Kassiotis, The concept of space and competition in immune regulation. *Immunology* **111**, 241-247 (2004).

17. G. Ferrari, H. Langen, M. Naito, J. Pieters, A coat protein on phagosomes involved in the intracellular survival of mycobacteria. *Cell* **97**, 435-447 (1999).
18. P. Mueller *et al.*, Regulation of T cell survival through coronin-1-mediated generation of inositol-1,4,5-trisphosphate and calcium mobilization after T cell receptor triggering. *Nat Immunol* **9**, 424-431 (2008).
19. N. Foger, L. Rangell, D. M. Danilenko, A. C. Chan, Requirement for coronin 1 in T lymphocyte trafficking and cellular homeostasis. *Science* **313**, 839-842 (2006).
20. M. K. Haraldsson *et al.*, The lupus-related Lmb3 locus contains a disease-suppressing Coronin-1A gene mutation. *Immunity* **28**, 40-51 (2008).
21. L. R. Shiow *et al.*, The actin regulator coronin 1A is mutant in a thymic egress-deficient mouse strain and in a patient with severe combined immunodeficiency. *Nat Immunol* **9**, 1307-1315 (2008).
22. J. Pieters, P. Muller, R. Jayachandran, On guard: coronin proteins in innate and adaptive immunity. *Nature reviews. Immunology* **13**, 510-518 (2013).
23. M. Okumura, C. Kung, S. Wong, M. Rodgers, M. L. Thomas, Definition of family of coronin-related proteins conserved between humans and mice: close genetic linkage between coronin-2 and CD45-associated protein. *DNA Cell Biol* **17**, 779-787 (1998).
24. B. Nal *et al.*, Coronin-1 expression in T lymphocytes: insights into protein function during T cell development and activation. *Int Immunol* **16**, 231-240 (2004).
25. K. Suzuki *et al.*, Molecular cloning of a novel actin-binding protein, p57, with a WD repeat and a leucine zipper motif. *FEBS Lett* **364**, 283-288 (1995).
26. R. Jayachandran *et al.*, Survival of mycobacteria in macrophages is mediated by coronin 1-dependent activation of calcineurin. *Cell* **130**, 37-50 (2007).
27. R. Jayachandran *et al.*, Coronin 1 regulates cognition and behavior through modulation of cAMP/protein kinase A signaling. *PLoS Biol* **12**, e1001820 (2014).
28. D. Suo *et al.*, Coronin-1 is a neurotrophin endosomal effector that is required for developmental competition for survival. *Nat Neurosci* **17**, 36-45 (2014).
29. P. Mueller, X. Liu, J. Pieters, Migration and homeostasis of naive T cells depends on coronin 1-mediated prosurvival signals and not on coronin 1-dependent filamentous actin modulation. *Journal of immunology* **186**, 4039-4050 (2011).
30. M. J. Lang, M. Mori, J. Ruer-Laventie, J. Pieters, A Coronin 1-Dependent Decision Switch in Juvenile Mice Determines the Population of the Peripheral Naive T Cell Compartment. *J Immunol* **199**, 2421-2431 (2017).
31. R. Jayachandran *et al.*, Disruption of Coronin 1 Signaling in T Cells Promotes Allograft Tolerance while Maintaining Anti-Pathogen Immunity. *Immunity* **50**, 152-165 e158 (2019).
32. M. Wang, C. J. Herrmann, M. Simonovic, D. Szklarczyk, C. von Mering, Version 4.0 of PaxDb: Protein abundance data, integrated across model organisms, tissues, and cell-lines. *Proteomics* **15**, 3163-3168 (2015).
33. T. Wolf *et al.*, Dynamics in protein translation sustaining T cell preparedness. *Nat Immunol* **21**, 927-937 (2020).
34. B. H. Luo, C. V. Carman, T. A. Springer, Structural basis of integrin regulation and signaling. *Annu Rev Immunol* **25**, 619-647 (2007).
35. D. G. Stupack, D. A. Cheresh, Get a ligand, get a life: integrins, signaling and cell survival. *J Cell Sci* **115**, 3729-3738 (2002).
36. A. M. Negulescu, P. Mehlen, Dependence receptors - the dark side awakens. *FEBS J* **285**, 3909-3924 (2018).

37. J. E. Meredith, Jr., M. A. Schwartz, Integrins, adhesion and apoptosis. *Trends Cell Biol* **7**, 146-150 (1997).
38. A. P. Gilmore, Anoikis. *Cell Death Differ* **12 Suppl 2**, 1473-1477 (2005).
39. D. Moshous *et al.*, Whole-exome sequencing identifies Coronin-1A deficiency in 3 siblings with immunodeficiency and EBV-associated B-cell lymphoproliferation. *J Allergy Clin Immunol* **131**, 1594-1603 (2013).
40. A. Misslitz, G. Bernhardt, R. Förster, Trafficking on serpentines: molecular insight on how maturing T cells find their winding paths in the thymus. *Immunological reviews* **209**, 115-128 (2006).
41. A. Hamann *et al.*, Evidence for an accessory role of LFA-1 in lymphocyte-high endothelium interaction during homing. *J Immunol* **140**, 693-699 (1988).
42. C. Berlin-Rufenach *et al.*, Lymphocyte migration in lymphocyte function-associated antigen (LFA)-1-deficient mice. *J Exp Med* **189**, 1467-1478 (1999).
43. P. Reichardt *et al.*, A role for LFA-1 in delaying T-lymphocyte egress from lymph nodes. *EMBO J* **32**, 829-843 (2013).
44. J. Gatfield, J. Pieters, Essential role for cholesterol in entry of mycobacteria into macrophages. *Science* **288**, 1647-1650 (2000).
45. R. Pick *et al.*, Coronin 1A, a novel player in integrin biology, controls neutrophil trafficking in innate immunity. *Blood* **130**, 847-858 (2017).
46. D. Suo, J. Park, S. Young, T. Makita, C. D. Deppmann, Coronin-1 and calcium signaling governs sympathetic final target innervation. *J Neurosci* **35**, 3893-3902 (2015).
47. T. Koike, D. P. Martin, E. M. Johnson, Jr., Role of Ca<sup>2+</sup> channels in the ability of membrane depolarization to prevent neuronal death induced by trophic-factor deprivation: evidence that levels of internal Ca<sup>2+</sup> determine nerve growth factor dependence of sympathetic ganglion cells. *Proc Natl Acad Sci U S A* **86**, 6421-6425 (1989).
48. P. A. Lampe, E. B. Cornbrooks, A. Juhasz, E. M. Johnson, Jr., J. L. Franklin, Suppression of programmed neuronal death by a thapsigargin-induced Ca<sup>2+</sup> influx. *J Neurobiol* **26**, 205-212 (1995).
49. E. L. de Hostos, B. Bradtke, F. Lottspeich, R. Guggenheim, G. Gerisch, Coronin, an actin binding protein of Dictyostelium discoideum localized to cell surface projections, has sequence similarities to G protein beta subunits. *EMBO J* **10**, 4097-4104 (1991).
50. A. F. Vinet *et al.*, Initiation of multicellular differentiation in Dictyostelium discoideum is regulated by coronin A. *Mol Biol Cell* **25**, 688-701 (2014).
51. W. F. Loomis, Cell signaling during development of Dictyostelium. *Dev Biol* **391**, 1-16 (2014).
52. C. H. Siu *et al.*, Regulation of spatiotemporal expression of cell-cell adhesion molecules during development of Dictyostelium discoideum. *Dev Growth Differ* **53**, 518-527 (2011).
53. T. Farinholt, C. Dinh, A. Kuspa, Social amoebae establish a protective interface with their bacterial associates by lectin agglutination. *Sci Adv* **5**, eaav4367 (2019).
54. W. R. Springer, D. N. Cooper, S. H. Barondes, Discoidin I is implicated in cell-substratum attachment and ordered cell migration of Dictyostelium discoideum and resembles fibronectin. *Cell* **39**, 557-564 (1984).
55. T. E. Crowley, W. Nellen, R. H. Gomer, R. A. Firtel, Phenocopy of discoidin I-minus mutants by antisense transformation in Dictyostelium. *Cell* **43**, 633-641 (1985).

56. M. Clarke, S. C. Kayman, K. Riley, Density-dependent induction of discoidin-I synthesis in exponentially growing cells of Dictyostelium discoideum. *Differentiation; research in biological diversity* **34**, 79-87 (1987).
57. C. Eckert, B. Hammesfahr, M. Kollmar, A holistic phylogeny of the coronin gene family reveals an ancient origin of the tandem-coronin, defines a new subfamily, and predicts protein function. *BMC evolutionary biology* **11**, 268 (2011).
58. A. Sebe-Pedros, A. J. Roger, F. B. Lang, N. King, I. Ruiz-Trillo, Ancient origin of the integrin-mediated adhesion and signaling machinery. *Proc Natl Acad Sci U S A* **107**, 10142-10147 (2010).
59. L. D. Hurst, C. Pal, M. J. Lercher, The evolutionary dynamics of eukaryotic gene order. *Nature reviews. Genetics* **5**, 299-310 (2004).
60. T. Takizawa, K. J. Meaburn, T. Misteli, The meaning of gene positioning. *Cell* **135**, 9-13 (2008).
61. E. Velardi, J. J. Tsai, M. R. M. van den Brink, T cell regeneration after immunological injury. *Nature Reviews Immunology* **21**, 277-291 (2021).
62. J. E. Jaspers, R. J. Brentjens, Development of CAR T cells designed to improve antitumor efficacy and safety. *Pharmacol Ther* **178**, 83-91 (2017).
63. D. W. Roadcap, C. S. Clemen, J. E. Bear, The role of mammalian coronins in development and disease. *Subcell Biochem* **48**, 124-135 (2008).
64. Y. Shinkai *et al.*, RAG-2-deficient mice lack mature lymphocytes owing to inability to initiate V(D)J rearrangement. *Cell* **68**, 855-867 (1992).
65. F. A. Ran *et al.*, Genome engineering using the CRISPR-Cas9 system. *Nat Protoc* **8**, 2281-2308 (2013).
66. A. Tulp, D. Verwoerd, B. Dobberstein, H. L. Ploegh, J. Pieters, Isolation and characterization of the intracellular MHC class II compartment. *Nature* **369**, 120-126 (1994).
67. V. Nedela, Methods for additive hydration allowing observation of fully hydrated state of wet samples in environmental SEM. *Microscopy research and technique* **70**, 95-100 (2007).
68. M. I. Love, W. Huber, S. Anders, Moderated estimation of fold change and dispersion for RNA-seq data with DESeq2. *Genome Biol* **15**, 550 (2014).
69. G. Yu, L. G. Wang, Y. Han, Q. Y. He, clusterProfiler: an R package for comparing biological themes among gene clusters. *OMICS* **16**, 284-287 (2012).
70. G. Yu, Q. Y. He, ReactomePA: an R/Bioconductor package for reactome pathway analysis and visualization. *Mol Biosyst* **12**, 477-479 (2016).
71. M. D. Robinson, D. J. McCarthy, G. K. Smyth, edgeR: a Bioconductor package for differential expression analysis of digital gene expression data. *Bioinformatics* **26**, 139-140 (2010).
72. A. Fabregat *et al.*, The Reactome Pathway Knowledgebase. *Nucleic Acids Research* **46**, D649-D655 (2018).
73. B. Gao, T. M. Curtis, F. A. Blumenstock, F. L. Minnear, T. M. Saba, Increased recycling of (alpha)5(beta)1 integrins by lung endothelial cells in response to tumor necrosis factor. *J Cell Sci* **113 Pt 2**, 247-257 (2000).
74. E. Ahrne *et al.*, Evaluation and Improvement of Quantification Accuracy in Isobaric Mass Tag-Based Protein Quantification Experiments. *J Proteome Res* **15**, 2537-2547 (2016).

75. Y. Wang *et al.*, Reversed-phase chromatography with multiple fraction concatenation strategy for proteome profiling of human MCF10A cells. *Proteomics* **11**, 2019-2026 (2011).
76. D. L. Plubell *et al.*, Extended Multiplexing of Tandem Mass Tags (TMT) Labeling Reveals Age and High Fat Diet Specific Proteome Changes in Mouse Epididymal Adipose Tissue. *Mol Cell Proteomics* **16**, 873-890 (2017).
77. Y. Perez-Riverol *et al.*, The PRIDE database resources in 2022: a hub for mass spectrometry-based proteomics evidences. *Nucleic Acids Research* **50**, D543-D552 (2022).

**Acknowledgments:** We thank Kai Schleicher (Imaging core facility, Biozentrum), Katarzyna Buczak (Proteomics Facility, Biozentrum); members of the Pieters laboratory for expert help and suggestions; Eva Bieler and Markus Dürrenberger (Swiss Nanoscience Institute/University of Basel, Biozentrum) for scanning electron microscopy; the patient and his family for their informed consent to support the research through blood donation; and Mrs. Michaela Corrias for logistics with blood transport. The P2A4 monoclonal antibody developed by E.A. Wayner and G. Vercellotti as well as the LFA-1 monoclonal antibodies (ITGAL clone TS1/22.1.1.13.3 and M17/4.4.11.9; ITGB2 clone H52, developed by Tim Springer) were obtained from the Developmental Studies Hybridoma Bank. We thank Li-Kuo Su (Life Science Editors) for critical reading.

**Funding:** This work was supported by a Cloëtta Foundation stipendium (to RJ), the European Union's Horizon 2020 research and innovation programme under the Marie Skłodowska-Curie grant agreement (to M.M., Grant number 800194), and grants from the Swiss National Science Foundation, the Swiss MS Society and the Canton of Basel (to JP). The scientific computing core facility at University of Basel obtains support from the Swiss Institute of Bioinformatics.

**Author Contributions:** T.N.F, C.B., R.J., J.R-L, M.M., A.S. and H.Z. performed experiments. T.N.F, C.B., A.S. G.F., J.P. analyzed data. D.M. provided reagents. T.N.F. and J.P. conceptualized and wrote the paper.

**Competing interests:** The authors declare that they have no competing interests.

**Data and materials availability:** The mass spectrometry proteomics data have been deposited to the ProteomeXchange Consortium via the PRIDE (77) partner repository with the dataset identifier PXD033997 and 10.6019/PXD033997 (<https://www.ebi.ac.uk/pride/archive/>). All other data needed to evaluate the conclusions in the paper are present in the paper or the Supplementary Materials. Data and code used in this paper are available upon request to JP.

## Figure Legends

### **Figure 1: Density-dependent T cell survival is promoted by coronin 1 in a T cell-intrinsic manner.**

(A) Coronin 1 protein levels in developing thymocytes from double negative (DN: CD4<sup>-</sup>CD8<sup>-</sup>) to double positive (DP: CD4<sup>+</sup>CD8<sup>+</sup>) to single positive medullary (SM: Qa2<sup>-</sup>CD62L<sup>-</sup>) to mature proliferation-competent single positive (M1: Qa2<sup>-</sup>CD62L<sup>lo</sup>) and to mature and emigration-competent single positive (M2: Qa2<sup>+</sup>CD62L<sup>+</sup>) thymocytes (n=5 animals per group).

(B) Percentage (population frequency) of T cells in WT mouse mesenteric lymph nodes (LN) compared to the spleen. \*\*\*\*\*, P <0.0001 by Student's t-test. n=5 animals per group.

(C) Coronin 1 protein levels in mature naive T cells from spleen and mesenteric lymph nodes (LN). \*\*\*\*\*, P <0.0001 by Student's t-test. n=5 animals per group.

(D) Distribution of protein abundances determined in Jurkat T cells (T=24 hr) using normalized spectral abundance factor (NSAF) as determined by mass spectrometry. The top 200 proteins are shaded light gray. The middle and right panels show magnified areas of the left panel with the same scale and y-axis. Middle: Coronin 1 expression at low density (rank 121; 0.5x10<sup>6</sup> cells/mL); right: coronin 1 expression in cells having reached high density (rank 11; 4x10<sup>6</sup> cells/mL). N=1 experiment with 3 technical replicates per group.

(E) T cells (Jurkat) were seeded at low density (2x10<sup>5</sup> cells/mL) and analyzed for cell growth at the times indicated. Shown is a representative result from 3 independent experiments.

(F,G) WT (F) or coronin 1-deficient (G) Jurkat T cells were seeded at 2x10<sup>5</sup> cells/mL and analyzed for caspase 3/7 (Casp 3/7) activity at the times indicated. N=2 independent experiments, each with 3 technical replicates per group.

(H) Proliferation of coronin 1-expressing and coronin 1-deficient Jurkat T cells (cl. 1 and cl. 2 are independently generated clones (out of ~20)) seeded at  $2 \times 10^5$  cells/mL and analyzed at the times indicated for cell numbers and viability by Trypan blue exclusion. Inset:

Percentages of viable cells in coronin 1-expressing or coronin 1-deficient Jurkat T cells seeded at  $2 \times 10^5$  cells/mL and analyzed at the times indicated for apoptosis. N>3 independent experiments, each with 3 technical replicates per group.

(I,J) Proliferation of coronin 1-expressing and coronin 1-deficient Jurkat T cells seeded at  $2 \times 10^5$  cells/mL, cultured for 72 hours, media swapped as described, and analyzed for numbers of live cells (I) and % viable cells (J) at the times indicated. Circles and squares represent growth in medium in medium conditioned by WT cells; triangles indicate growth in medium conditioned by coronin 1-deficient cells. N=3 independent experiments, each with 3 technical replicates per group.

(K,L) WT and coronin 1-deficient Jurkat T cells were seeded ( $2 \times 10^5$  cells/mL) in culture separately or at WT:*Cor1*<sup>-/-</sup> ratios of 20:80 (WT:KO\_20/80), 40:60 (WT:KO\_20/80), 80:20 (WT:KO\_20/80) and analyzed by FACS at the indicated times for coronin 1 immunofluorescence and viability. The means  $\pm$  standard deviation of the percentages of coronin 1-expressing cells (K) and viability (L) are shown. N=2 independent experiments, each with 3 technical replicates per group.

**Figure 2: Coronin 1-modulated surface expression of LFA-1 and ICAM1 regulates density-dependent cell death initiation**

(A) Heatmap of significant differentially expressed genes with functions related to adhesion pathways in WT and coronin 1-deficient mouse T cells (31). Normalized variance stabilized transformation (vst) expression values calculated in DESeq2 and hierarchically clustered using Pearson correlation with average linkage as implemented in R.

**(B)** Dot plot showing the most significantly enriched pathways among the differentially expressed genes in WT and coronin 1-deficient conventional T cells for the Reactome Pathways collection. P-values were adjusted using the Benjamini-Hochberg procedure. The background set of genes (universe) was the 14427 genes detected in the RNA-seq experiments.

**(C)** Mouse T cells were isolated from spleen and cultured for 24 hours at  $2 \times 10^7$  cells/ml prior to imaging. Images are representative of multiple fields per well (technical triplicates) of T cells from at least 3 animals per group. Bar: 100  $\mu\text{m}$ .

**(D)** Cell surface expression of ICAM1, ITGAL and ITGB2 on mouse naïve T cells ( $\text{CD3}^+\text{CD4}/8^+\text{CD24}^-\text{CD62L}^{\text{hi}}\text{CD44}^{\text{lo}}$  or  $\text{CD3}^+\text{CD4}/8^+\text{CD24}^-\text{CD62L}^{\text{hi}}\text{Qa2}^{\text{hi}}\text{CD44}^{\text{lo}}$ ) as analyzed by flow cytometry. Plots are representative of at least 4 independent experiments, each with samples from  $\geq 3$  animals per group.

**(E)** WT or coronin 1-deficient Jurkat T cells seeded at  $2 \times 10^5$  cell/mL in the culture medium supplemented with propidium iodide to visualize dead cells, imaged at the indicated time points. Images are representative of  $N > 4$  independent experiments, each with 3 technical replicates per group. Scale bar: 500  $\mu\text{m}$ . See also Movies S1 and S2.

**(F)** TUNEL stained sections of mouse spleen and lymph nodes: Nuclei are in blue and apoptotic cells are in red. Images are representative of sections from 3 spleens and  $\geq 9$  inguinal and axillary lymph nodes from 3 animals per group. Scale bar: 500  $\mu\text{m}$  (top), 50  $\mu\text{m}$  (bottom).

**(G-H)** Brightfield images (G) and cell viability (H) of WT and coronin 1-deficient Jurkat T cell cultures seeded at  $2 \times 10^5$  cells/mL without or with the indicated function blocking antibody and cultured for 4 days. Scale bar: 200  $\mu\text{m}$ , Error bar: standard deviation.  $N = 5$  independent experiments, each with 3 technical replicates per group. \*\*\*\*,  $P < 0.0001$  by two-way ANOVA.

**Figure 3: Coronin 1 controls T cell population size by inducing LFA-1 internalization to suppress cell death signaling mediated by surface LFA-1**

(A) Surface expression of ICAM1 and LFA-1 on naive CD4 human T cells of a subject with homozygous coronin 1 destabilizing V134M mutation compared to healthy donor. Median fluorescence intensity (MFI) is shown. N=3 technical replicates per subject.

(B) Schematic outline of the experimental workflow for adoptive transfer of mouse T cells treated with DPBS, anti-LFA-1 (M17) or the isotype control (GK3) into *Rag2*<sup>-/-</sup> mice (B). Percentage of WT T cells in blood 2 days after adoptive transfer into *Rag2*<sup>-/-</sup> mice (left) and total number of T cells recovered from spleen, inguinal lymph nodes and blood at day 4 (right) (C). T cell counts per organ following the treatments indicated are shown (D). Data from n≥3 mice per group obtained in 3 independent experiments are shown.

(E-G) Schematic workflow showing Jurkat T cells maintained in culture at low density ( $\leq \sim 5 \times 10^5$  cells/mL) or allowed to expand to high density ( $\geq \sim 2 \times 10^6$  cells/mL) for 24 hrs before re-seeding at increasing density (E). Cell density-dependent MFI of surface ITGB2 (F) and viability (G) are plotted for Jurkat T cells re-seeded from low and high density cultures as indicated. N=3 independent experiments, each with 3 technical replicates per group. Graphs show means  $\pm$  standard deviation. ns, not statistically significant, \*\*\*, P<0.001 \*\*\*\*, P<0.0001 by one-way ANOVA in (F) and (G).

(H) FACS analysis of integrin ITGB2 cell surface levels (gray bars) and cell viability (Live/Dead marker, pink bars) after seeding of Jurkat T cells at  $8 \times 10^6$  cells/mL at the times indicated. S/T: surface to total ratio. N=2 independent experiments, with 3 technical replicates per group.

(I) Immunofluorescence images of coronin 1 (red) and ITGB2 (green) in Jurkat cells and the corresponding DIC images are shown. Arrowheads indicate apposition of coronin 1 with

ITGB2. Images are representative of 2 independent experiments, each with >40 cells per group.

(J) Kinetics of the internalization of ITGB2 from cell surface to intracellular space as determined by flow cytometry of surface-internalized ITGB2. N=2 independent experiments, each with 3 technical replicates per group.

**Figure 4: Coronin 1-dependent prosurvival Ca<sup>2+</sup> mobilization is cell-density and LFA1-dependent**

(A) Intracellular Ca<sup>2+</sup> release upon PLC stimulation in WT and coronin 1-deficient Jurkat T cells maintained at low density ( $\leq \sim 5 \times 10^5$  cells/mL) or cultured to high density ( $\geq \sim 2 \times 10^6$  cells/mL). N=3 independent experiments, each with 3 technical replicates per group.

(B) Viability of WT and coronin 1-deficient Jurkat cells seeded at  $2 \times 10^5$  cells/mL with or without thapsigargin (Tg) at the indicated concentration and sampled at 120h. Means  $\pm$  standard deviation are shown. N=2 independent experiments, each with 4 technical replicates per group. ns: not statistically significant, \*\*\*\*,  $P < 0.0001$  by one-way ANOVA.

(C) Intracellular Ca<sup>2+</sup> release upon PLC stimulation in WT and coronin 1-deficient Jurkat T cells cultured to high density ( $\geq \sim 2 \times 10^6$  cells/mL) with LFA-1 function blocking antibody (H52). N=2 independent experiments, each with 2 technical replicates per group.

**Figure 5: An evolutionarily conserved coronin-dependent pathway regulates cell density-dependent survival through kin-to-kin cell adhesion signaling**

(A) WT, coronin A-deficient (*corA*<sup>-</sup>) or coronin A-deficient complemented with FLAG-tagged coronin A (*corA*<sup>-</sup>/*FLAG* -*CorA*) *Dictyostelium discoideum* were seeded at  $10^5$

cells/mL and cell numbers analyzed at the times indicated. N=3 independent experiments, each with 3 technical replicates per group. \*\*\*\*\*, P <0.0001 by one-way ANOVA.

(B) Heat maps of mass spectrometry-determined log<sub>2</sub>ratio of density-dependent significantly regulated proteomes of wild type and *corA*<sup>-</sup> at late lag (24h), early log (48h) and early stationary (110h) growth phase. Cells that had been maintained in culture through at least 4 passages at lag-phase density (always below 8x10<sup>5</sup> cell/mL) were re-seeded at 10<sup>5</sup> cells/mL and analyzed by mass spectrometry at the indicated time points. 148 proteins of 4301 total proteins identified by mass spectrometry were determined to be significantly regulated in coronin A- and cell density-dependent manner. Representative of the average of 3 technical replicates per group.

(C) Enrichment analysis and functional annotation of the top 148 proteins that were significantly regulated during different phases of growth between WT and *corA*<sup>-</sup> *Dictyostelium* cells (see also Data File S5).

(D) Most significantly enriched known proteins from (B) and (C) are shown.

(E) Example set of proteins that increase in abundance in WT or *corA*<sup>-</sup>/FLAG-*CorA* *Dictyostelium discoideum* upon reaching high cell density but are already significantly increased in *corA*<sup>-</sup> *Dictyostelium discoideum* at low cell density. Symbols as in (A).

(F) Example set of proteins that significantly decrease in abundance in WT or *corA*<sup>-</sup>/FLAG-*CorA* *Dictyostelium discoideum* upon reaching high cell density but are already significantly reduced in *corA*<sup>-</sup> *Dictyostelium discoideum* at low cell density. Symbols as in (A).

**Figure 6: Model depicting the role for coronin 1/coronin A in cell population size control while maintaining cellular individuality**

Upper: During cell population increase, coronin 1 (in T cells) or coronin A (in *Dictyostelium*) abundance (green) is modulated according to cell density increase, thereby dampening

adhesion molecule-initiated cell population growth arrest and/or death signaling (red). Lower left: Whereas coronin is dispensable for cell population density increase at low cell densities, in its absence the threshold at which growth arrest/death signaling is initiated far below the threshold at which WT cells regulate their cell density. Lower right: This role for coronin 1/coronin A to coordinate homotypic sensing with cell population density also allows the maintenance of cellular individuality.

# Figure 1

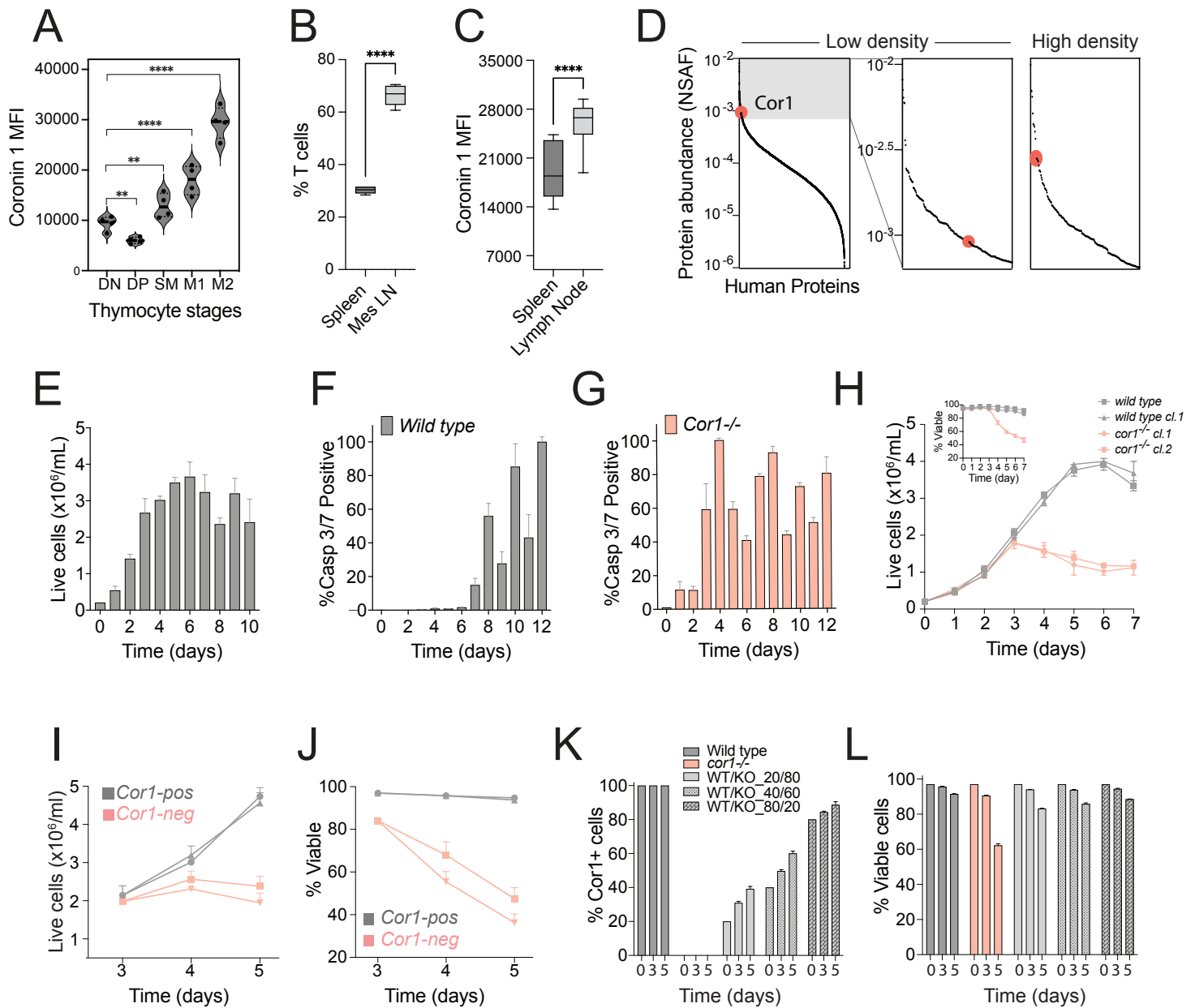


**Figure 1: Density-dependent T cell survival is promoted by coronin 1 in a cell-intrinsic manner.**

**(A)** Expression of coronin 1 mRNA determined by RNAseq in wild type double negative thymocytes (DN) and splenic mature naive T (MNT) cells (data from (14)); Shown are mean + standard deviation; P-values were determined by student t-test, \*\*\*\*: <math><0.0001</math>,  $n=6$  animals.

**(B)** Coronin 1 protein levels in mature naive T cells from spleen and mesenteric lymph nodes (LN); P-values were determined by Student t-test, \*\*\*\*: <math><0.0001</math>,  $n=8$  animals.

**(C)** Percentage (population frequency) of T cells in mouse lymph nodes compared to the spleen; P-values were determined by Student's t-test, \*\*\*\*: <math><0.0001</math>,  $n=5$  animals. The P-values in (C-E) for the day 5 time point were determined by two-way ANOVA:  $p < 0.0001$ .

**(D)** Distribution of protein abundances determined in Jurkat T cells ( $T=24$  hr) using normalized spectral abundance factor (NSAF) as determined by mass spectrometry. The top 200 proteins are shaded light gray. Middle panel: coronin 1 expression at low density (rank 121;  $0.5 \times 10^6$  cells/mL); right panel: coronin 1 expression in cells having reached high density (rank 11;  $4 \times 10^6$  cells/mL).

**(E)** T cells (Jurkat) were seeded at  $2 \times 10^5$  cells/mL, and analyzed for cell growth at the times indicated.

**(F,G)** Wild type (F) or coronin 1-deficient (G) Jurkat T cells were seeded at  $2 \times 10^5$  cells/mL, and analyzed for caspase 3/7 activity at the times indicated.

**(H)** Proliferation of coronin 1-expressing and coronin 1-deficient Jurkat T cells seeded at  $2 \times 10^5$  cells/mL and analyzed at the times indicated for cell numbers and viability (by Trypan blue exclusion, see inset for % viable cells). The coronin 1-deficient cells are easily disaggregated by gentle repeated pipetting. Inset: Percentages of viable cells in coronin 1-expressing or coronin 1-deficient Jurkat T cells seeded at  $2 \times 10^5$  cells/mL and analyzed at the times indicated for apoptosis.

**(I,J)** Proliferation of coronin 1-expressing and coronin 1-deficient Jurkat T cells seeded at  $2 \times 10^5$  cells/mL, cultured for 72 hours, media swapped as described and analyzed at the times indicated. Circles and squares represent growth in wild type conditioned medium; triangles indicate growth in conditioned medium from coronin 1-deficient cells.

**(K,L)** Co-culture of wild type and coronin 1-deficient Jurkat cells: wild type and coronin 1-deficient Jurkat T cells were seeded ( $2 \times 10^5$  cells/mL) in culture separately or at wild type:cor1-/- ratios of 20:80 (WT:KO\_20/80), 40:60 (WT:KO\_40/60), 80:20 (WT:KO\_80/20) and sampled at indicated times and stained coronin 1 as well as viability then analyzed by FACS. The mean + standard deviation of the percentages of coronin 1-expressing cells (K) and viability (L) are shown.

# Figure 2

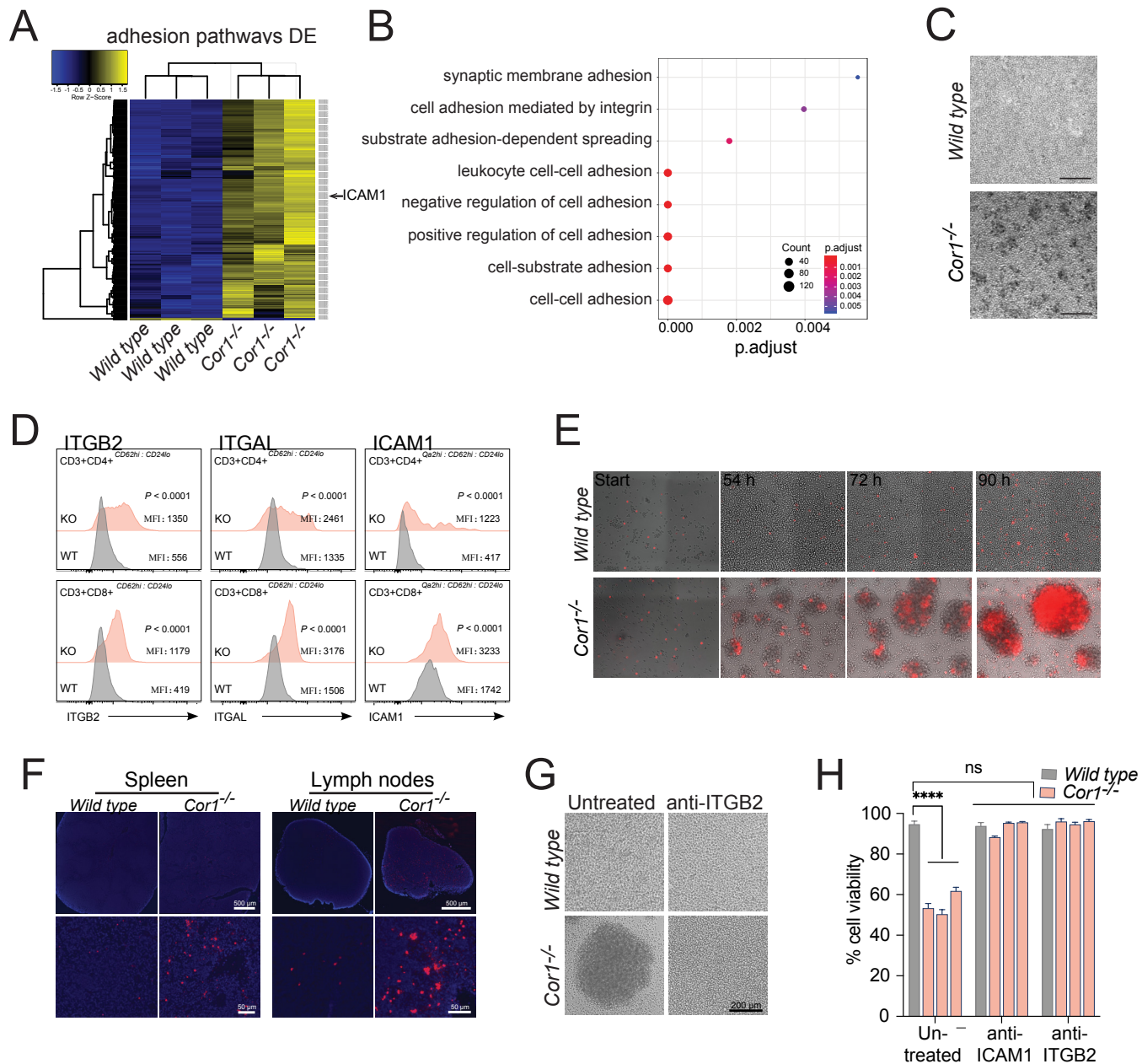


**Figure 2: Coronin 1-modulated LFA-1/ICAM1 surface expression regulates density-dependent cell death initiation**

**(A)** Heatmap of significant differentially expressed genes with function related to adhesion pathways in wild type and coronin 1-deficient mouse T cells. Regularized log-transformed (rlog) expression values calculated in DESeq2 and hierarchically clustered using Pearson correlation with average linkage as implemented in R. Cor1: coronin 1.

**(B)** Dot plot showing the most significantly enriched pathways among the differentially expressed genes in wild type versus coronin 1-deficient conventional T cells for the Reactome Pathways collection. P-values were adjusted using the Benjamini-Hochberg procedure. The background set of genes (universe) was the ~15000 genes detected in the RNA-Seq experiments.

**(C)** Mouse T cells were isolated from spleen and cultured for 24 hours at  $2 \times 10^7$  cells/ml prior to imaging. Bar: 100  $\mu$ m.

**(D)** Cell surface expression of ICAM1, ITGAL and ITGB2 on mouse naive T cells as analyzed by flow cytometry. Median fluorescence intensity (MFI) and P-values for  $n \geq 4$  of at least 4 independent experiments are indicated.

**(E)** Time sequence images of wild type or coronin 1-deficient Jurkat T cells seeded at  $2 \times 10^5$  cell/mL in the presence of propidium iodide, to visualize dead cells, at the indicated time points. See also suppl movie 1 and 2.

**(F)** TUNEL stained sections of mouse spleen and lymph nodes: Nuclei in blue and apoptotic cells in red.

**(G-H)** Function blocking LFA-1/ICAM1: (g) brightfield images and (h) cell viability of wild type and coronin 1-deficient Jurkat T cell culture seeded at  $2 \times 10^5$  cells/mL without or with function block antibody and cultured for 4 days. Scale bar: 200  $\mu$ m, Error bar: standard deviation. Representative data of 5 independent experiments are shown.

Figure 3

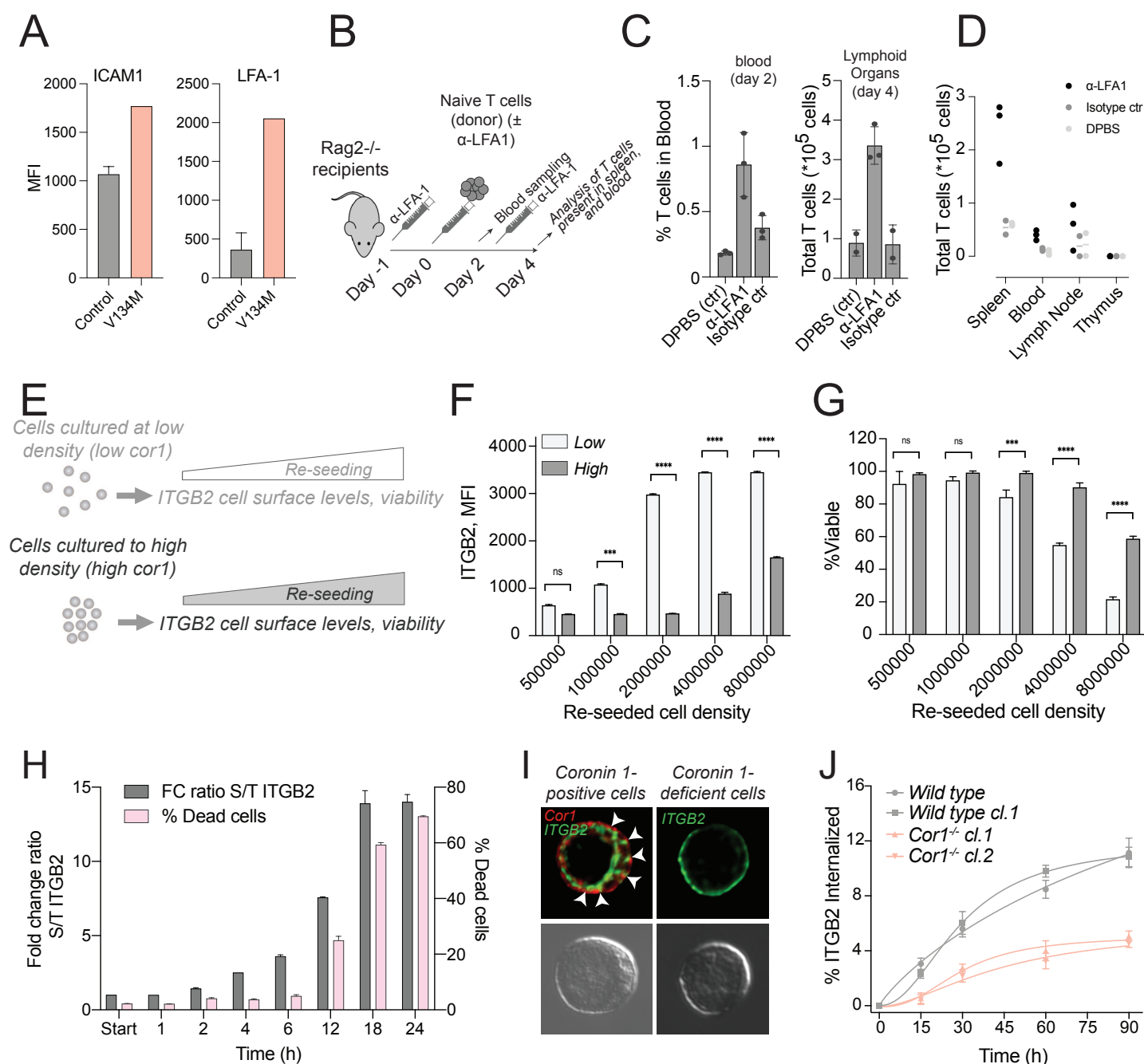


**Figure 3: Coronin 1 regulates T cell population homeostasis by moderating surface LFA-1-mediated cell death signalling through LFA-1 internalization.**

(A) Surface expression of ICAM1 and LFA-1 on naive CD4 human T cells of a subject with homozygous coronin 1 destabilizing V134M mutation compared to control donor: Median fluorescence intensity (MFI) are plotted.

(B-D) In vivo reversal of T cell death by anti-LFA-1 function blocking antibody: (B) Schematic outline of the experimental workflow for adoptive transfer of mouse T cells in Rag2<sup>-/-</sup> treated with DPBS, anti-LFA-1 (M17) or the isotype control (GK3). (C) Percentage of wild type T cells in blood 48 hrs after adoptive transfer into Rag2<sup>-/-</sup> mice (left) and total number of T cells recovered from spleen, axillary lymph nodes and blood after 96 hrs (right). In (D), T cell counts per organ following the treatments indicated are shown. Representative data from 3 independent experiments are shown, n≥2.

(E-G) Density shock experiment: (E) Schematic workflow showing Jurkat T cells maintained in culture at low density (≤ ~5x10<sup>5</sup> cells/mL) or allowed to expand to high density (≥ ~2x10<sup>6</sup> cells/mL) for 24 hrs. before re-seeding at increasing density. Cell density-dependent MFI of surface ITGB2 (F) and viability (G) are plotted for Jurkat T cells re-seeded from low and high density cultures as indicated.

(H) Analysis of integrin ITGB2 cell surface levels by FACS (gray bars) and cell viability (Trypan blue exclusion, pink bars) following seeding of Jurkat T cells at 8x10<sup>6</sup> cells/mL at the times indicated. S/T: surface to total ratio.

(I) Subcellular distribution of ITGB2 in wild type and coronin 1-deficient Jurkat T cells: Immunofluorescence images of coronin 1 (red) and ITGB2 (green) and the corresponding DIC images are shown. Arrowheads indicate apposition of coronin 1 with ITGB2.

(J) Kinetics of the internalization of ITGB2 from cell surface to intracellular space as determined by flow cytometry of surface-internalized ITGB2. All graphs show the mean + standard deviation: n≥3; P-values were determined by student t-test (A and B) and two-way ANOVA (D): ns>0.05; \*\*\*\*: <0.0001.

Figure 4

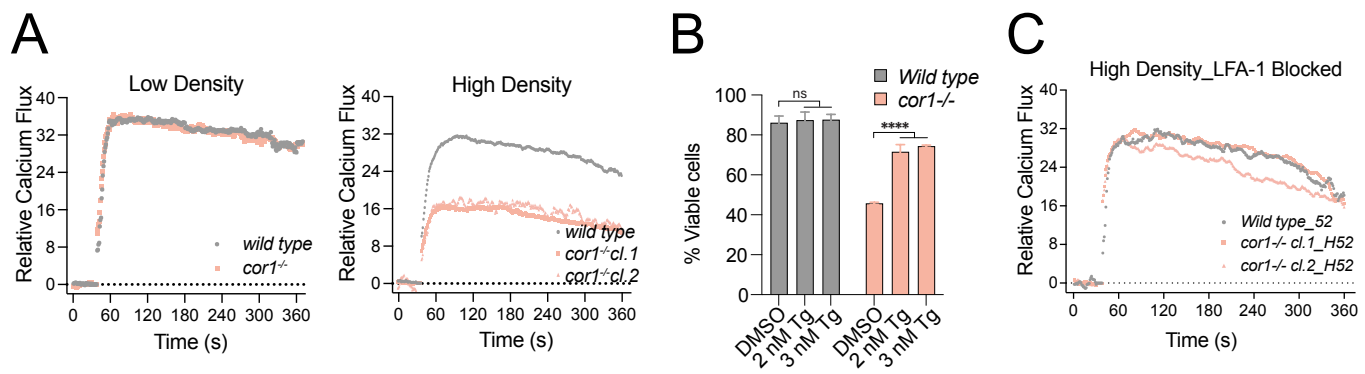


**Figure 4: Coronin 1-dependent prosurvival Ca<sup>2+</sup> mobilization is cell-density and LFA1-dependent**

**(A)** Intracellular calcium release upon PLC stimulation in wild type and coronin 1-deficient Jurkat T cells maintained at low density ( $\leq \sim 5 \times 10^5$  cells/mL) or cultured to high density ( $\geq \sim 2 \times 10^6$  cells/mL).

**(B)** Viability of wild type and coronin 1-deficient Jurkat cells seeded at  $2 \times 10^5$  cells/mL with or without thapsigargin (Tg) at the indicated concentration and sampled at 120h; Shown are mean + standard deviation:  $n=4$ ; P-values were determined by two-way ANOVA: ns:  $>0.1$ ; \*\*\*\*:  $<0.0001$ .

**(C)** Intracellular calcium release upon PLC stimulation in wild type and coronin 1-deficient Jurkat T cells cultured to high density ( $\geq \sim 2 \times 10^6$  cells/mL) with LFA-1 function block antibody (H52).

# Figure 5

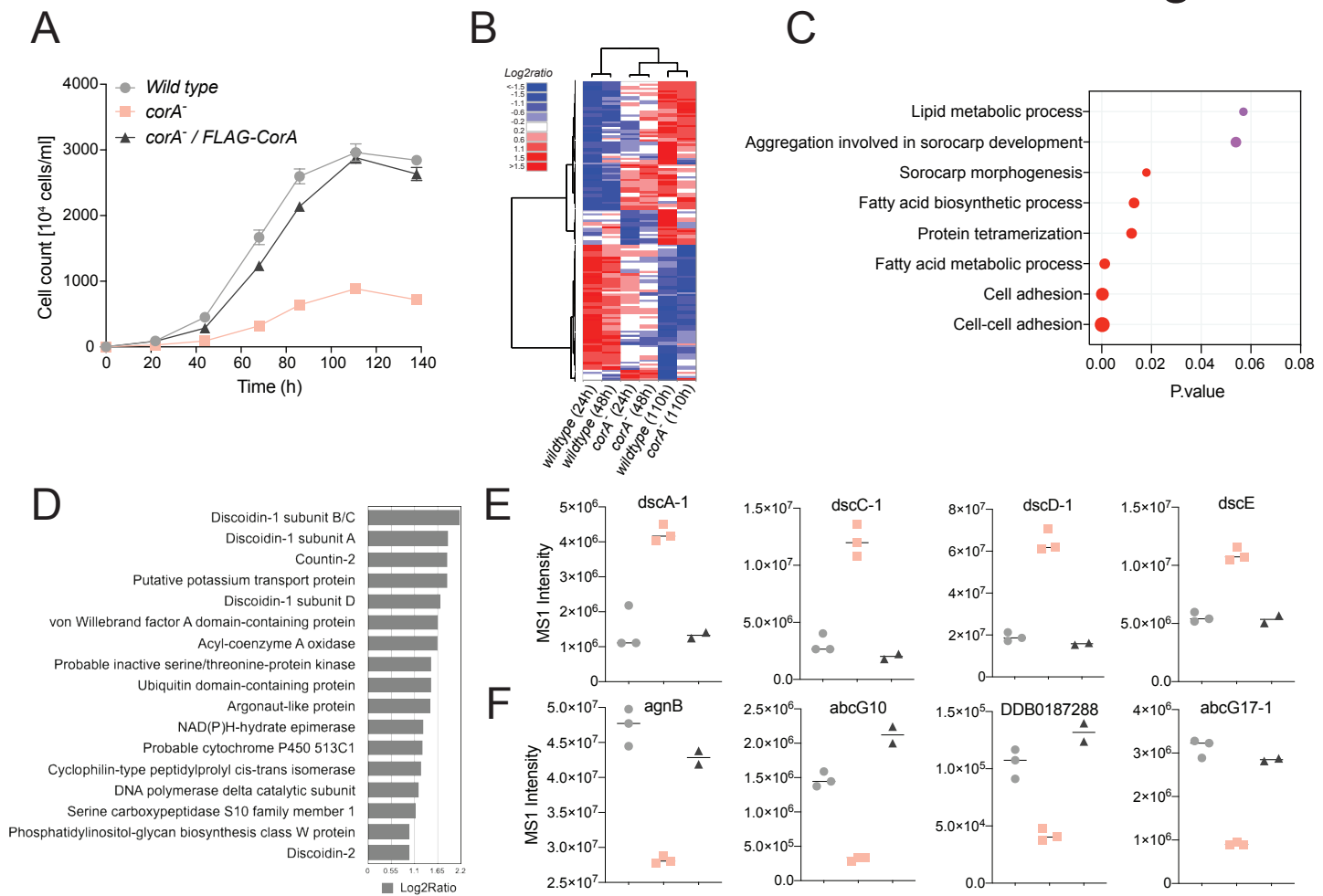


**Figure 5: An evolutionary conserved coronin-dependent pathway regulates cell density-dependent survival through homeostatic kin-to-kin cell adhesion signaling.**

**(A)** Wild type, coronin A-deficient (*corA*<sup>-</sup>) or coronin A-deficient complemented with FLAG-tagged coronin A (*corA*<sup>-</sup>/FLAG-CorA) *Dictyostelium discoideum* were seeded at  $10^5$  cells/mL and cell numbers analyzed at the times indicated. The P-values for the 140 h time point were determined by two-way ANOVA: \*\*\*\*: <math><0.0001</math>.

**(B)** Intracellular calcium release upon PLC stimulation in wild type and coronin 1-deficient Jurkat T cells maintained at low density ( $\leq 5 \times 10^5$  cells/mL) or cultured to high density ( $\geq 2 \times 10^6$  cells/mL). b, Viability of wild type and coronin 1-deficient Jurkat cells seeded at  $2 \times 10^5$  cells/mL with or with thapsigargin (Tg) at the indicated concentration and sampled at 120h; Shown are mean + standard deviation: n=4; P-values were determined by two-way ANOVA: ns: >0.1; \*\*\*\*: <math><0.0001</math>. c, Intracellular calcium release upon PLC stimulation in wild type and coronin 1-deficient Jurkat T cells cultured to high density ( $\geq 2 \times 10^6$  cells/mL) with LFA-1 function block antibody (H52). Heat maps of mass spectrometry-determined log2ratio of density-dependent significantly regulated proteomes of wild type and *corA*<sup>-</sup> at late lag (24h), early log (48h) and early stationary (110h) growth phase. Cells that had been maintained in culture through at least 4 passages at lag-phase density (always below  $8 \times 10^5$  cell/mL) were re-seeded at  $10^5$  cells/mL and sampled at the indicated time points for mass spectrometry. 148 proteins of 4301 total proteins identified by mass spectrometry were determined to be significantly regulated in *corA*<sup>-</sup> and cell density-dependent manner.

**(C)** Enrichment analysis and functional annotation of the top 148 proteins that were significantly regulated during different phases of growth between wild type and *corA*<sup>-</sup> *Dictyostelium* cells (see also Table S5).

**(D)** Most significantly enriched proteins from Panel B,C. Shown are known proteins only.

**(E)** Example set of proteins that increase in abundance in wild type or *corA*<sup>-</sup>/FLAG-CorA upon reaching high cell density but are already significantly increased in *corA*<sup>-</sup> at low cell density.

**(F)** Example set of proteins that significantly decrease in abundance in wild type or *corA*<sup>-</sup>/FLAG-CorA upon reaching high cell density but are already significantly reduced in *corA*<sup>-</sup> at low cell density.

Figure 6

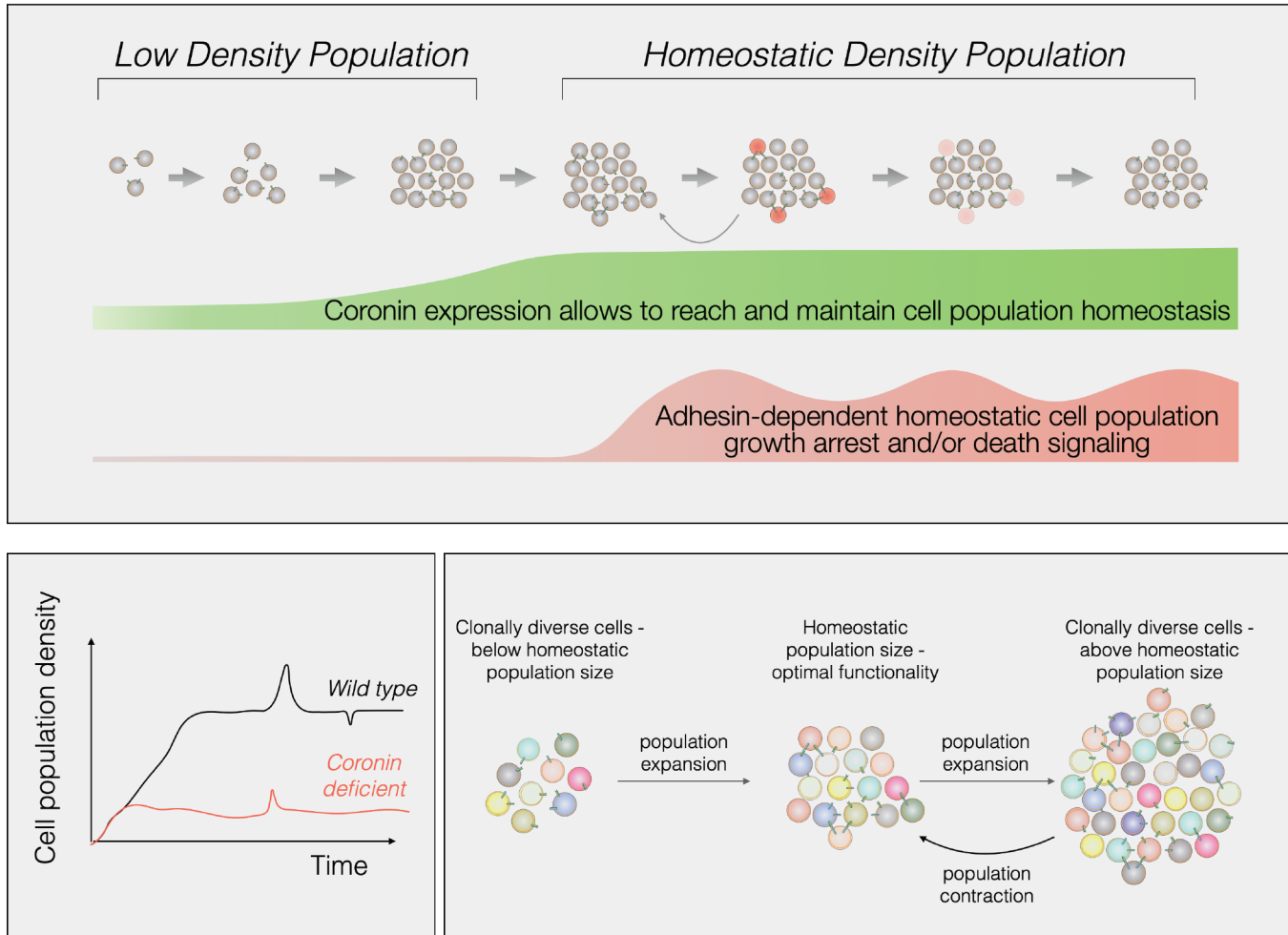


**Figure 6: Model depicting the role for coronin 1/A in cell population homeostasis and maintaining cellular individuality**

Upper panel: During cell population increase, coronin 1/A expression (green) is tuned to cell density increase, thereby dampening adhesin-initiated cell population growth arrest and/or death signaling (red). Lower left: Whereas at low cell densities, coronin is dispensable for cell population density increase, in its absence the threshold at which growth arrest/death signaling is initiated is far below the threshold at which wild type cells regulate their cell density. Lower right: This role for coronin 1A to coordinate kin-to-kin sensing with cell population density also allows the maintenance of cellular individuality.